



**AFRL-RY-WP-TR-2010-1163**

**MEASUREMENT AND GENERATION OF ULTRA-HIGH  
POWER FIBER LASER PULSES BY COHERENT  
COMBINATION**

**Pamela Bowlan and Rick Trebino**

**Swamp Optics LLC**

**JUNE 2010  
Final Report**

**Approved for public release; distribution unlimited.**

*See additional restrictions described on inside pages*

**STINFO COPY**

**AIR FORCE RESEARCH LABORATORY  
SENSORS DIRECTORATE  
WRIGHT-PATTERSON AIR FORCE BASE, OH 45433-7320  
AIR FORCE MATERIEL COMMAND  
UNITED STATES AIR FORCE**

## NOTICE AND SIGNATURE PAGE

Using Government drawings, specifications, or other data included in this document for any purpose other than Government procurement does not in any way obligate the U.S. Government. The fact that the Government formulated or supplied the drawings, specifications, or other data does not license the holder or any other person or corporation; or convey any rights or permission to manufacture, use, or sell any patented invention that may relate to them.

This report was cleared for public release by the Defense Advanced Research Projects Agency's Public Release Center and is available to the general public, including foreign nationals. Copies may be obtained from the Defense Technical Information Center (DTIC) (<http://www.dtic.mil>).

AFRL-RY-WP-TR-2010-1163 HAS BEEN REVIEWED AND IS APPROVED FOR PUBLICATION IN ACCORDANCE WITH ASSIGNED DISTRIBUTION STATEMENT.

\*//Signature//

---

BRYCE SCHUMM, Chief  
Coherent LADAR Section  
Laser Radar Technology Branch

\*//Signature//

---

BRIAN D. EWERT, Chief  
LADAR Technology Branch  
Multispectral Sensing & Detection Division

\*//Signature//

---

TRACY W. JOHNSTON, Chief  
Multispectral Sensing & Detection Division  
Sensors Directorate

This report is published in the interest of scientific and technical information exchange, and its publication does not constitute the Government's approval or disapproval of its ideas or findings.

\*Disseminated copies will show “//Signature//” stamped or typed above the signature blocks.

<b>REPORT DOCUMENTATION PAGE</b>				<i>Form Approved</i> OMB No. 0704-0188	
The public reporting burden for this collection of information is estimated to average 1 hour per response, including the time for reviewing instructions, searching existing data sources, gathering and maintaining the data needed, and completing and reviewing the collection of information. Send comments regarding this burden estimate or any other aspect of this collection of information, including suggestions for reducing this burden, to Department of Defense, Washington Headquarters Services, Directorate for Information Operations and Reports (0704-0188), 1215 Jefferson Davis Highway, Suite 1204, Arlington, VA 22202-4302. Respondents should be aware that notwithstanding any other provision of law, no person shall be subject to any penalty for failing to comply with a collection of information if it does not display a currently valid OMB control number. <b>PLEASE DO NOT RETURN YOUR FORM TO THE ABOVE ADDRESS.</b>					
<b>1. REPORT DATE (DD-MM-YY)</b> June 2010		<b>2. REPORT TYPE</b> Final		<b>3. DATES COVERED (From - To)</b> 13 May 2009 – 12 May 2010	
<b>4. TITLE AND SUBTITLE</b> MEASUREMENT AND GENERATION OF ULTRA-HIGH POWER FIBER LASER PULSES BY COHERENT COMBINATION				<b>5a. CONTRACT NUMBER</b> FA8650-09-C-7933	
				<b>5b. GRANT NUMBER</b>	
				<b>5c. PROGRAM ELEMENT NUMBER</b> 69199F	
<b>6. AUTHOR(S)</b> Pamela Bowlan and Rick Trebino				<b>5d. PROJECT NUMBER</b> ARPR	
				<b>5e. TASK NUMBER</b> YJ	
				<b>5f. WORK UNIT NUMBER</b> ARPRYJOE	
<b>7. PERFORMING ORGANIZATION NAME(S) AND ADDRESS(ES)</b> Swamp Optics LLC 6300 Powers Ferry Rd. #600-345 Atlanta, GA 30339-2919				<b>8. PERFORMING ORGANIZATION REPORT NUMBER</b>	
<b>9. SPONSORING/MONITORING AGENCY NAME(S) AND ADDRESS(ES)</b> Air Force Research Laboratory Sensors Directorate Wright-Patterson Air Force Base, OH 45433-7320 Air Force Materiel Command United States Air Force				<b>10. SPONSORING/MONITORING AGENCY ACRONYM(S)</b> AFRL/RYSJM	
				<b>11. SPONSORING/MONITORING AGENCY REPORT NUMBER(S)</b> AFRL-RY-WP-TR-2010-1163	
<b>12. DISTRIBUTION/AVAILABILITY STATEMENT</b> Approved for public release; distribution unlimited.					
<b>13. SUPPLEMENTARY NOTES</b> DARPA DISTAR Case 15859; Clearance Date: 26 July 2010. This report contains color.					
<b>14. ABSTRACT</b> In this seedling project, we studied the feasibility of coherently combining the output beams of multiple pulse-seeded fiber-optical amplifiers. Our procedure was to begin with a nanosecond seed pulse from a micro-disk laser, amplify it, and then develop a device to measure it in order to determine whether the pulses produced by currently available fiber-laser sources are sufficiently stable and possess sufficiently clean waveforms that it is conceivable that they can be combined coherently. As a result, we developed new single-shot frequency-resolved-optical gating (FROG) pulse-measurement techniques with unprecedented spectral resolution and temporal range, with the ability to measure potentially extremely complex pulses on a single shot. Using this technology, we studied the pulses produced by an Yt-fiber-amplified micro-disk laser. Although we found that the pulse shape became somewhat complex as amplification increased, we believe that the phase stability was sufficient.					
<b>15. SUBJECT TERMS</b> Ytterbium laser amplifier; YDFA; fiber lasers; nanosecond pulse; frequency-resolved optical gating (FROG)					
<b>16. SECURITY CLASSIFICATION OF:</b>			<b>17. LIMITATION OF ABSTRACT:</b> SAR	<b>18. NUMBER OF PAGES</b> 50	<b>19a. NAME OF RESPONSIBLE PERSON (Monitor)</b> Bryce Schumm <b>19b. TELEPHONE NUMBER (Include Area Code)</b> N/A
<b>a. REPORT</b> Unclassified	<b>b. ABSTRACT</b> Unclassified	<b>c. THIS PAGE</b> Unclassified			

# Table of Contents

<u>Section</u>	<u>Page</u>
List of Figures .....	ii
List of Tables .....	iv
1. Executive Summary .....	1
2. Introduction.....	2
3. Nanosecond MOPA .....	4
4. Absolute Phase Stability Measurements.....	8
5. Nanosecond Pulse Intensity-and-Phase Measurements .....	11
5.1 Frequency Resolved Optical Gating .....	11
5.2 Etalon Spectrometer .....	13
5.2.1 Introduction.....	13
5.2.2 Testing the Etalon Spectrometer.....	13
5.2.3 Measuring the Free Spectral Range of the VIPA etalons .....	15
5.3 Multi-Shot ns-FROG .....	18
5.4 Nanosecond Pulse-Front Tilt (PFT).....	21
5.4.1. Introduction.....	21
5.4.2. Modeling the Spatiotemporal Field of the Pulse From a VIPA Etalon .....	23
5.4.3. Measuring the Spatiotemporal Field of the Pulse From a VIPA Etalon.....	24
5.4.4 Results and Discussion .....	26
5.5 Single-Shot ns-FROG .....	27
5.5.1 Experimental setup.....	27
5.5.2 Testing the FROG.....	29
5.5.3 Measuring Amplified Pulses.....	30
5.6 Elegant Single-Shot ns-FROG.....	31
5.6.1 New Experimental Setup .....	31
5.6.2 Testing the Elegant Single-Shot ns-FROG .....	33
5.6.3 Measurement Range of Our Single-Shot ns-FROG.....	34
5.6.4 Measuring amplified pulses .....	35
6. Conclusions.....	39
7. References.....	40
List of Acronyms, Abbreviations, and Symbols .....	42

## List of Figures

<b><u>Figure</u></b>	<b><u>Page</u></b>
Figure 1. Schematic of Our MOFA .....	5
Figure 2. Measured properties of our MOFA .....	6
Figure 3. Proposed schematic for coherent combination using the MOFA in Figure 1 .....	7
Figure 4. Interferometer for measuring the absolute phase of the amplified pulse relative to the seed pulse .....	8
Figure 5. Interferograms at different pump power levels .....	9
Figure 6. The phase drift for an amplified pulse of 140mW and for 400 mW .....	10
Figure 7. Schematic of a FROG (frequency-resolved autocorrelation) apparatus [6] .....	11
Figure 8. Etalon spectrometer .....	14
Figure 9. Simulations of the output of our etalon spectrometer .....	14
Figure 10. Experimental setup for testing and calibrating the VIPA spectrometer .....	15
Figure 11: Spectra measured with the etalon spectrometer .....	15
Figure 12. Measuring the spectral response function of our 532nm etalon spectrometer .....	16
Figure 13. Temporal response (left) and spectral response (right) of our 1cm thick 532nm etalon .....	17
Figure 14. Measuring the line width of the 5mm, 1064nm VIPA etalon .....	17
Figure 15. Measuring the line width of the 1cm, 1064nm VIPA etalon.....	18
Figure 16. Schematic of our multi-shot FROG.....	18
Figure 17. FROG measurement and retrieval results of the pulses from the Standa microchip laser .....	19
Figure 18. FROG measurement and retrieval results for a 1.77 ns double pulse .....	20
Figure 19. Prisms and diffraction gratings introduce angular dispersion, or, if viewed in time, pulse front tilt.....	21
Figure 20. Schematic of the tilted pulse front that emerges from a “VIPA” etalon .....	22
Figure 21. Retrieving the spatio-spectral field of the unknown pulse from the interferogram ....	24
Figure 22. Experimental setup for measuring the spatiotemporal field of the pulse from an etalon .....	25
Figure 23. Measurement (top) and simulation (bottom) of the spatiotemporal field after a VIPA etalon.....	26
Figure 24. Our 1 <sup>st</sup> version of the single-shot ns-FROG .....	28
Figure 25. FROG measurement of the seed laser (a) and a 3ns double pulse (b).....	29
Figure 26. High-resolution spectra (~0.09pm) of the amplified pulse at different pump power levels .....	30
Figure 27. FROG retrieval results for the amplified seed pulse with 8 (a) and 12 times gain (b) .....	31
Figure 28. Final version of our single-shot ns-FROG .....	32
Figure 29. Generating two spatially overlapping oppositely tilted pulse fronts .....	32
Figure 30. FROG measurement results for a single pulse (a) and a double pulse (b) .....	33
Figure 31. FROG measurements of 3ns (top), a 2.56ns (middle), and a 2ns double pulse (bottom) .....	34
Figure 32. FROG traces of pulses from the Yb fiber amplifier for different pump power levels .....	35
Figure 33. FROG retrieval results for 12× (a) and 15× amplification (b) .....	36

<b><u>Figure</u></b>	<b><u>Page</u></b>
Figure 34. Single shot spectra of the amplified pulses at 3 different pump powers .....	37
Figure 35. Single-shot FROG traces of an amplified pulse .....	37
Figure 36. Retrievals for two different single shot FROG measurements.....	38

## List of Tables

<u>Table</u>	<u>Page</u>
Table 1. Output parameters for the seed laser and the amplifier .....	5
Table 2. Summary of pulses measurable with the single-shot ns-FROG. ....	34

# 1. Executive Summary

Pulsed fiber lasers are potentially ideal for many real world applications because they are small, compact and relatively insensitive to environmental conditions. But, unfortunately, compared with solid-state lasers, they are fundamentally limited to lower power levels. As a result, there has been much recent effort to *coherently combine* the output of several lasers into one, potentially resulting in much higher pulse energy. While this has been accomplished for cw lasers, it has never been done for pulses as short as a nanosecond or less, or even for pulses shorter than microseconds.

The purpose of our project was to determine whether or not coherent combination of nanosecond pulses is even feasible. The main questions, is whether or not each pulse from an amplifier is the same, or how rapidly the pulses changes. If the pulses are very complex and change drastically from shot-to-shot—especially in phase—then it may not be possible to combine the outputs of two separate amplifiers into one pulse. Answering this question involves measuring the nanosecond pulse's shape, as well as its phase (or the arrival time of its various colors), and for each pulse individually. Because these pulses may have structure that is shorter than the fastest electronic response times, there was no way to make this measurement. Worse, measuring the phase is even more difficult.

This report describes our result from a year long project to develop suitable diagnostics to determine whether or not coherent combination of nanosecond pulses is feasible. We first built a simple single-stage master oscillator fiber amplifier starting with seed pulses with a 720ps duration and  $\sim 8\mu\text{J}$  of energy and using a large-mode-area Yb fiber to amplify them. To measure the pulses, we extended a technique for measuring femtosecond pulses called frequency-resolved optical gating (FROG) to the nanosecond regime. Using our seed laser, we developed first a multi-shot ns-FROG, and then later came up with what we consider to be a very clever (much more clever than that in our original proposal) scheme to make it operate single-shot. We describe in detail the operation of our nanosecond FROGs and show measurements demonstrating that they work well.

Once we had successfully developed the necessary diagnostics (i.e. the single-shot ns-FROG) we used it to study the amplified pulses from our Yb fiber. Using the FROG trace, we observed in real time the emergence of nonlinearities as the pump power was increased. A broadening of the pulse's spectrum and shortening of the pulse duration from 720ps to  $\sim 250\text{ps}$  was observed. Also, with enough amplification we were able to measure individual pulses from the amplified pulse train and confirm that their temporal shape and phase were the same for every pulse. This is a very promising result for coherent combination.

In conclusion, this report illustrates that our FROG device is a powerful tool for achieving coherent combination of nanosecond pulses. In fact it will be useful for measuring nanosecond pulses in general, which are widely used in research, defense, and industry. We have only scratched the surface of interesting and useful measurements that could be made with it.

## 2. Introduction

Fiber lasers are potentially ideal for defense applications, having the potential to be operated at high power levels. Nonetheless, peak and average powers larger than those currently available are needed. Fundamental limitations prevent simply scaling existing designs to higher powers. An alternative approach, which we explored in this project, is to coherently combine the outputs of multiple fiber laser sources.

This seedling project was a feasibility study of coherently combining the output beams of multiple pulse-seeded fiber-optical amplifiers. The goal of our research was to determine whether the construction of such a laser source is feasible and to uncover possible hidden challenges to the construction of such a source. Specifically we sought to measure both the *intensity* and *phase* of individual pulses in the amplified pulse train. When we began this work, there was no method for measuring such pulses, typically in the 100ps to 10ns range.

Therefore, our project had three main goals: To construct a high-power pulsed seeded fiber amplifier, to develop a method to measure the intensity and phase of 100ps to 10ns pulses in a single shot, and then to use this method to measure the our amplified pulses. Our twelve-month milestones were the following:

- Measure the complete intensity and phase of the Telesto or similar laser's pulse.
- Confirm FROG measurements using an alternative method, either temporal interferometry (TI) or spectral interferometry (SI).
- Perform more exacting measurements of the phase-preservation characteristics of the commercial and developmental ytterbium-doped fiber-amplifier (YDFA) modules. These measurements will be performed initially by monitoring the beat note between the input and output wave forms (temporal interferometry) and later by using the FROG apparatus (and SI, if necessary).
- Complete the construction of the two YDFA modules.

In this report we discuss all of the work performed for this project in order to achieve these goals.

When we began, our first task was to design and build a nanosecond master oscillator fiber amplifier. This is described in section 3. Once we had constructed a working amplifier, we made some basic measurements of its performance, such as its output power versus pump power, and the spatial profile, which are shown in Section 3. We also measured its ability to preserve the absolute phase, which we discuss in Section 4. Section 5 discusses the bulk of our work, which involved inventing, developing, and testing a completely novel, and quite clever, device to measure both the intensity and phase of pulses >100ps to 4ns long on a single-shot. Our device is based on a general and robust method for measuring femtosecond pulses called FROG. We went through several versions of this device as we simplified and improved it. We did most of the initial development of our measurement devices using our seed laser, but after the nanosecond FROG was working well, we studied the amplified pulses, observed the nonlinearities, and confirmed that minimal shot-to-shot variations were occurring.

In conclusion we think that our FROG device will be a powerful for tool for achieving coherent combination of nanosecond pulses and for measuring nanosecond pulses in general.

### 3. Nanosecond MOPA

The first task of this project was to design a suitable master oscillator fiber amplifier (MOFA). This serves as our test laser for investigating the pulse intensity and phase shot-to-shot stability of a typical fiber MOFA and also as the light source for designing and testing our ns-FROG. Our goal was to reach a peak power of around 50-100kW ( $\sim 100\mu\text{J}$ ).

To design an amplifier that best suits our needs, there are several requirements. First of all, since a high peak power and coherent combination are the goals, it is best to make the pulse's temporal intensity and phase (the arrival time of the colors) as simple as possible. Also, the fewer stages of amplification used, the more simple and more stable the output pulses will likely be. And for achieving coherent combination, it seems best to start with a single seed laser, which is then split into several channels, or amplifiers, and the outputs of these amplifiers can be combined. Therefore we want to start with an intense, but still compact, seed laser that emits near-transform-limited pulses.

Also, it is actually more difficult to amplify a nanosecond pulse than it is a slightly sub-nanosecond pulse. This is because nanosecond pulses have line widths very similar to the stimulated Brillouin scattering line width of ytterbium-doped fiber (50-100MHz) making this nonlinear process favorable so that the pulses become distorted in the amplifier. Another difficulty with amplifying nanosecond pulses is that the front of the pulse experiences more gain than the back of the pulse, so the seed has to be pre-shaped to cancel out this effect in order to obtain a Gaussian pulse out of the amplifier [1]. If the pulse duration is less than 1ns, then the gain reshaping is probably negligible so that no pre-shaping is necessary.

We explored several options for a seed laser, such as pulsed diode lasers and continuous-wave (cw) lasers in combination with electro-optic modulators to make them pulsed. But nanosecond pulsed diode lasers emit very complicated pulses, with much more bandwidth than is needed ( $\sim 40$  times) to generate sub-10ns pulses. Generating nanosecond pulses by slicing a cw laser would produce quite weak pulses that would need many stages of amplification, and a very fast modulator and function generator would be needed.

Therefore we decided to instead use a passively Q-switched Nd:LSB microchip laser as the seed for the MOFA (see for example [2]). Microchip lasers typically have cavity lengths of less than a mm, are diode pumped, and a saturable absorber can be used as one of the end mirrors to generate pulses. Microchip lasers are well known for their spectral purity and typically emit transform-limited pulses as short as  $\sim 100\text{ps}$  or as long as  $\sim 1\text{ns}$  with several  $\mu\text{J}$  of energy per pulse. We decided to use the microchip laser sold by Standa, which has a repetition rate of 10kHz, a pulse duration of 500ps, a 3pm linewidth, and  $7.5\mu\text{J}$  per pulse, which is similar to what was used for the MOFA shown in references [3-5]. The price of this laser is about  $1/4^{\text{th}}$  of a pulsed diode laser (\$8,000), and it has about 100 times more energy, and shorter, transform-limited pulses. The disadvantages of using a microchip laser are that they are not as stable (0.4% energy fluctuation) as pulsed diode lasers and their repetition rate and pulse duration are not easily tunable. Nevertheless, it turned out to be perfect for our project, especially since the seed laser without any amplification was intense enough to test our FROG.

Starting with 7.5 $\mu$ J in the seed pulse also vastly simplifies the amplifier. To meet the goals of this project, we used only one stage of amplification. The MOFA that we built was inspired by reference [5], and is shown in Figure 1.

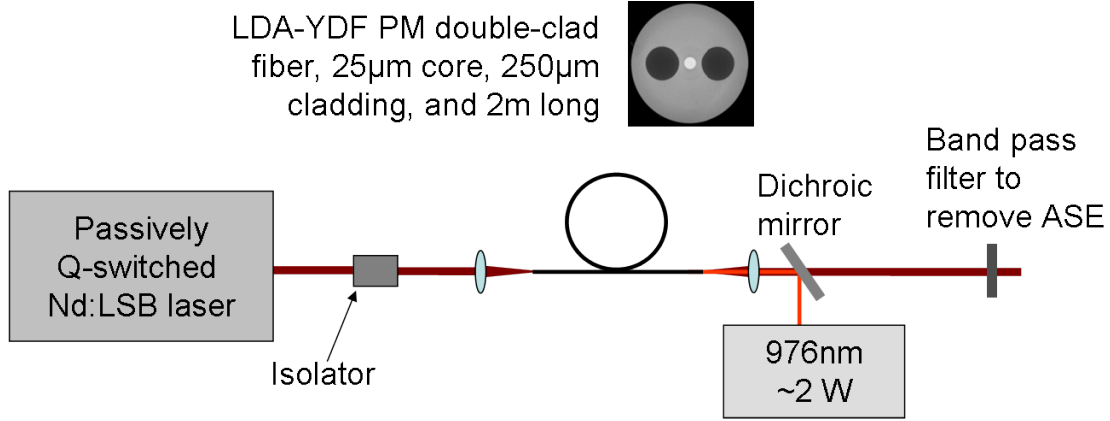


Figure 1. Schematic of Our MOFA

The Standa seed laser has a collimated output, and we first send this through a free-space isolator to protect the laser from back reflections. As the gain fiber, we use a large mode area, double clad Ytterbium fiber with a core diameter of 25 $\mu$ m (NA = 0.05), cladding diameter of 250  $\mu$ m (NA = 0.46), and a fiber length of 2m. We backward pump the Yb fiber using a collimated diode laser (from Apollo Instruments) at a wavelength of 976nm and with a line width of about 3nm. Backward pumping decreases the effective interaction length and minimizes nonlinearities [5]. For flexibility, we used a pump laser that emits up to 35W, although only ~1-3W were used for the single amplifier. The expected pulse parameters for our amplifier are shown in Table 1.

Table 1. Output parameters for the seed laser and the amplifier

	Seed laser microchip laser	Output pulses
<b>Center wavelength</b>	1064 nm	1064 nm
<b>Peak power</b>	15kW	>150 kW
<b>Average power</b>	82 mW	>820 mW
<b>Pulse duration</b>	650 ps	650 ps
<b>Pulse repetition frequency</b>	10 kHz	10 kHz
<b>Line width</b>	3 pm (transform limited)	3 pm
<b>Energy per pulse</b>	7.5 $\mu$ J	>75 $\mu$ J

Some of the measured characteristics of our MOFA are shown in Figure 2.

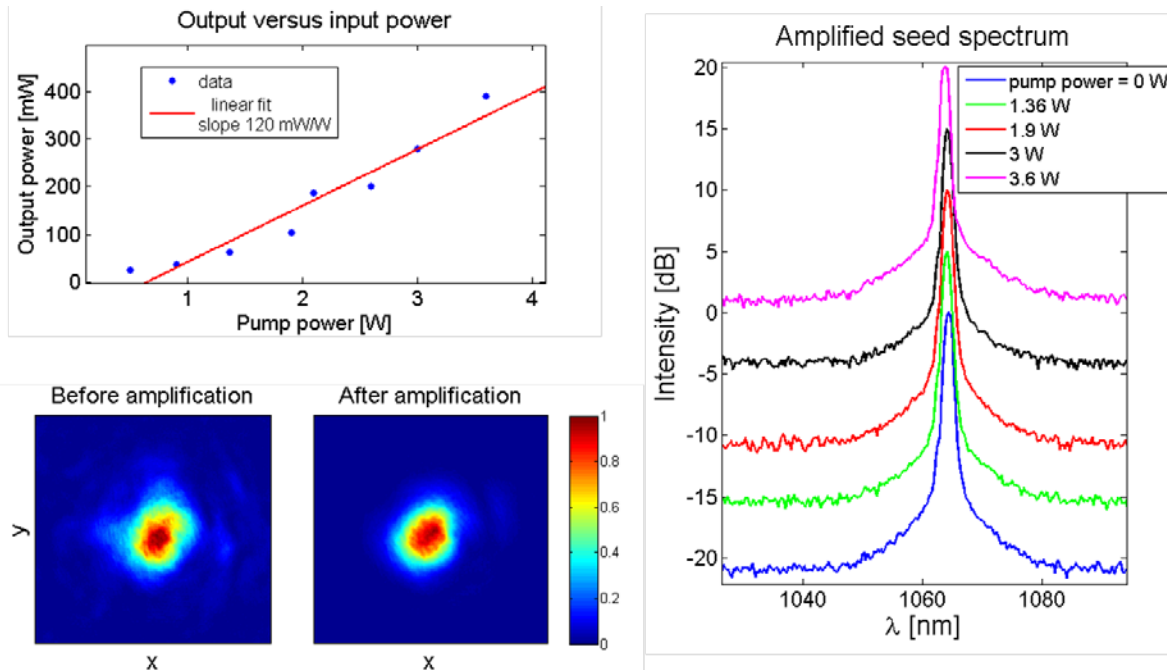


Figure 2. Measured properties of our MOFA

The top right plot shows the pump power needed to achieve a given output power in the amplified seed. Note that some of this pump power was lost due to coupling and at the dichroic beam splitter. The most output power that we have achieved so far is 380mW, which corresponds to a gain of 20 or 13dB when comparing the power emitted by the fiber with and without pump light. The bottom left plot shows the spatial profile of the beam before and after amplification, which indicates close to single-mode operation of the fiber. Because some of the input light is coupled into the outer core, but this light is not amplified, the spatial profile actually looks better after amplification. The plot at the right shows low resolution ( $\sim 0.1$  nm) spectra of output pulses from the fiber amplifier for different pump powers, which we measured to look for signs of nonlinearities. But later we measured higher resolution spectra, which show the spectrum changing even for  $<1$ W of pump power.

Although not part of this project, we wanted to make sure that our amplifier could easily be constructed to have several channels that could be coherently combined. The figure below illustrates one possible scheme for adding additional channels to our MOFA.

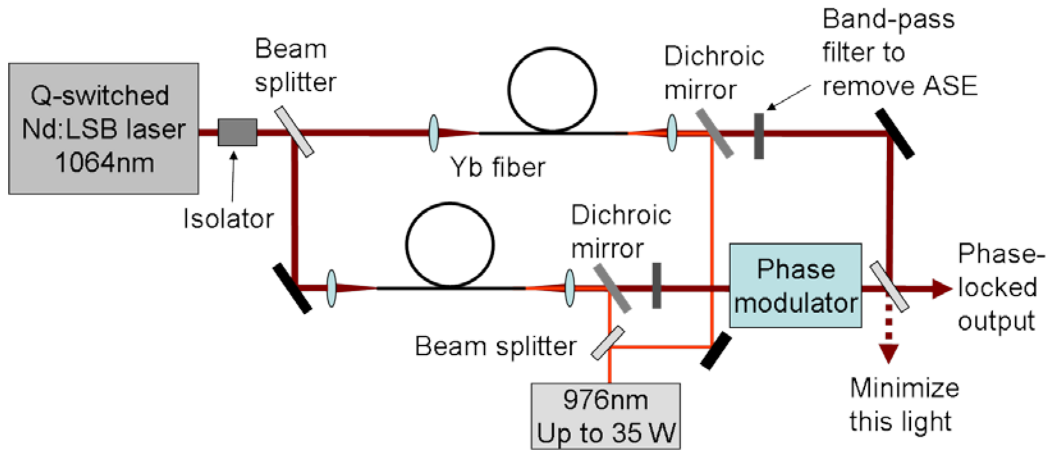


Figure 3. Proposed schematic for coherent combination using the MOFA in Figure 1

## 4. Absolute Phase Stability Measurements

One of the objectives of this project was to study the ability of the Yb amplifier to preserve the absolute phase of the seed pulse. It is important to determine how fast and by how much the absolute phase of the amplified pulse varies to determine the best approach for coherently combining the output of two separate amplifiers. With our FROG measurements (see the next section), we can determine all of the temporal characteristics of the pulse except for the absolute phase and the arrival time of the pulse (in other words, all higher-order terms of the spectral and temporal phases are determined, as well as the intensities). While the arrival time is not expected to vary significantly on the time scale of the pulse length and so need not be carefully measured, we do require another method for measuring the absolute phase of the amplified seed pulse.

Any type of interference can be used to determine the absolute-phase difference between the interfering beams (and to a lesser extent the pulse arrival time). To determine the phase difference between the amplified and seed pulses, we pick off a little of the seed pulse before the fiber amplifier and then cross this beam at a small angle with the amplified beam at a CCD camera. Crossing the two beams results in spatial interference fringes, whose phase (or the locations of the maxima) depends on the relative phase of the interfering pulses:

$$I_{interference}(x, y) = \left| E_{seed}(x, y) + E_{amp}(x, y) \right|^2 = \left| E_{seed}(x, y) \right|^2 + \left| E_{amp}(x, y) \right|^2 + 2 \left| E_{seed}(x, y) E_{amp}(x, y) \right| \cos(kx\theta + \Delta\varphi_{absolute}), \quad (1)$$

where  $\theta$  is the crossing angle and  $k$  is the wave number. A schematic of the experimental setup that we used to make these measurements is shown in Figure 4. The image at the bottom right shows an example of what the measured interference fringes look like.

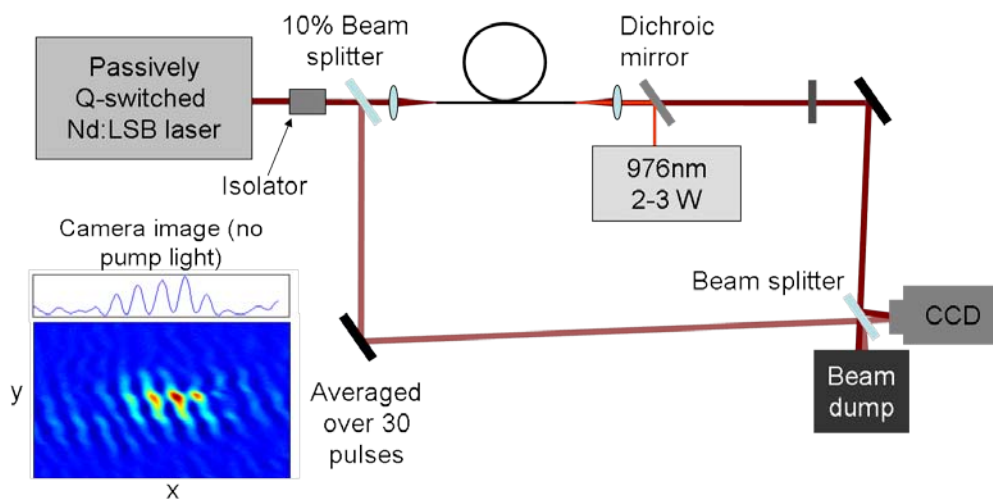


Figure 4. Interferometer for measuring the absolute phase of the amplified pulse relative to the seed pulse

To temporally overlap the seed and amplified pulses, we have to propagate the seed pulse in free space to make up for the 2m of gain fiber. This delay line introduces some of its own phase drifts so that these measurements only give us an upper bound on the phase drift of the amplifier itself. A better measurement would be to interfere the outputs of two different Yb amplifiers.

There are two ways that we can use these measurements to determine the phase stability of the amplifier relative to the seed. As the phase drifts, the maxima of the fringes move. So with an exposure time for the camera that averages over multiple pulses, the drifting phase will result in a smearing out or loss of contrast of the fringes. Or if the fringe contrast is perfect, then so is the phase stability. Figure 5 shows the measured interference patterns for three different amounts of amplification.

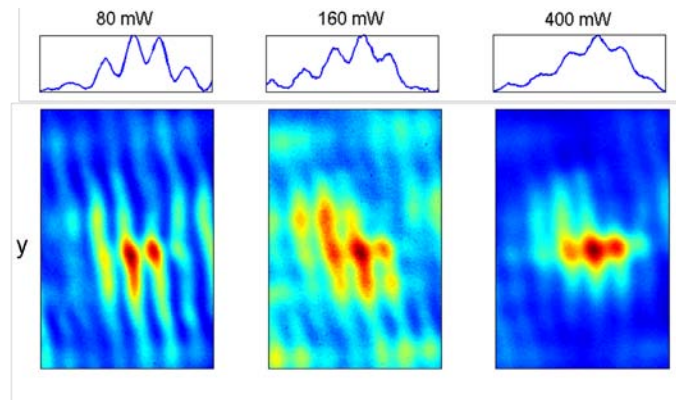


Figure 5. Interferograms at different pump power levels

The interferograms in Figure 5 were averaged over 30 pulses and it is easy to see that the fringe contrast decreased as we increased the amount of amplification. This indicates that the phase drift is becoming faster and larger with more amplification. But many things can affect the fringe contrast including the relative amplitudes, polarization, temporal pulse shape, center frequency, spatial phase and intensity of the interfering pulses in addition to their relative phases. Therefore studying the coherence between the pulses using the fringe contrast requires matching all of these additional quantities for the interfering pulses, which we tried to do in these preliminary measurements, but this is difficult.

Instead, a better approach is to directly extract the phase drift versus time from interferograms by making repeated measurements and tracking the maxima in the fringes. To extract the phase of the fringes, we Fourier transformed the interferograms to the  $k$ -domain, where the phase at the center of either of the side bands (much like the Fourier filtering used in spectral interferometry) is the relative phase between the interfering pulses. These results are shown below.

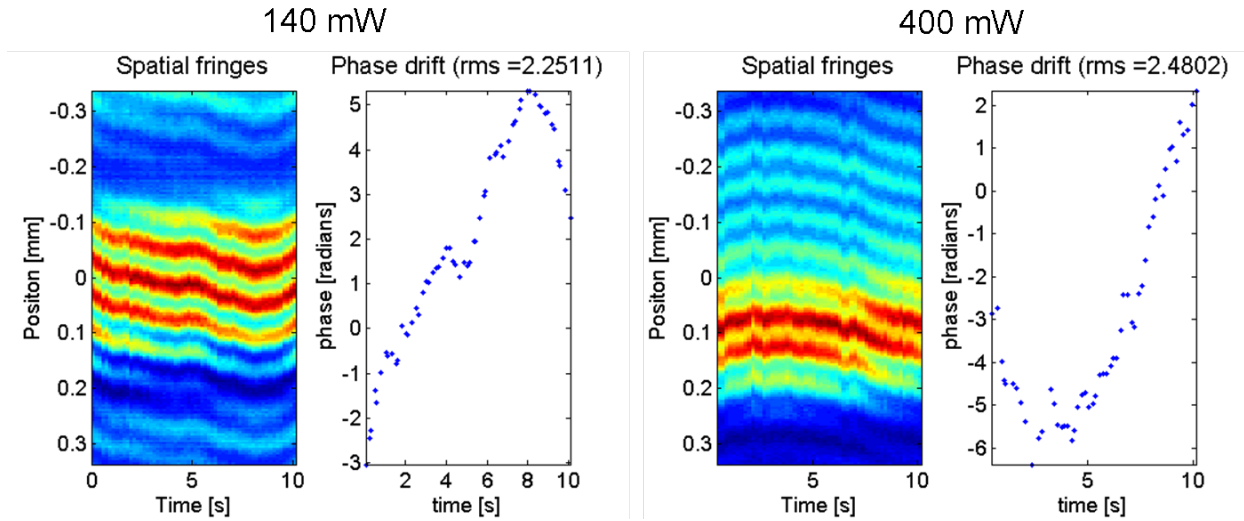


Figure 6. The phase drift for an amplified pulse of 140mW and for 400 mW

We first performed this measurement with no amplification to test the stability of the interferometer, and we found the rms phase drift over 10s to be 1 radian. In Figure 6 the spatial fringes (a cut through the center of the two-dimensional interferogram) and the extracted relative phase drift versus time are shown for two different amounts of amplification. For each interferogram we averaged over 30 laser pulses (3 ms). These data show that the phase drift of our amplifier is slow and small, and therefore should be easy to compensate for with a phase modulator, which would allow coherent combination of two amplifiers. When we increased the amplification by 2.8 times, the rms phase drift only increased by  $\sim 0.2$  radians. We expect that adding more pump energy to the amplifier, so that non-linear effects are likely, will make the phase drift much faster and larger.

## 5. Nanosecond Pulse Intensity-and-Phase Measurements

In order to coherently combine the output of ns-fiber lasers, it is first necessary to develop methods to measure and monitor these pulses. In particular, we must be able to measure the pulse intensity and phase vs. time. And we must do so on a single shot—averaging over many shots does not yield useful information because the coherent combination will necessarily occur on every shot, individually. Unfortunately, the measurement of nanosecond pulses with potentially picosecond structure is currently an unsolved problem. Such pulses are too short (too broadband) to be easily measured in the time domain and too long (too narrowband) to be easily measured in the frequency domain. So we developed a method to measure them in the time-frequency domain using a relatively long-pulse version of a well established time-frequency-domain technique for measuring femtosecond pulses: frequency-resolved optical gating (FROG).

In this section we will first give a general description the FROG technique, and discuss the challenges for extending it to measure nanosecond pulses. Next we will describe and show our results for high-resolution virtual-image phase array (VIPA) etalon spectrometers, which are necessary for making FROG measurements of nanosecond-pulses.

### 5.1 Frequency Resolved Optical Gating

FROG involves time-gating the pulse with itself and measuring the gated chunk of the pulse, as in autocorrelation. But unlike autocorrelation, it involves measuring the *spectrum* vs. the delay between the two pulses, and not just the energy. The general expression for a FROG trace is:

$$I_{FROG}(\omega, \tau) = \left| \int_{-\infty}^{\infty} E_{sig}(t, \tau) \exp(-i\omega t) dt \right|^2, \quad (2)$$

where the signal field,  $E_{sig}(t, \tau)$ , is a function of time and delay, usually of the form  $E_{sig}(t, \tau) = E(t) E_{gate}(t - \tau)$ . In FROG, the gate function,  $E_{gate}(t)$ , is a function of the unknown input pulse,  $E(t)$ , that we are trying to measure. When using second-harmonic generation (SHG) as the nonlinear-optical process,  $E_{gate}(t) = E(t)$ .

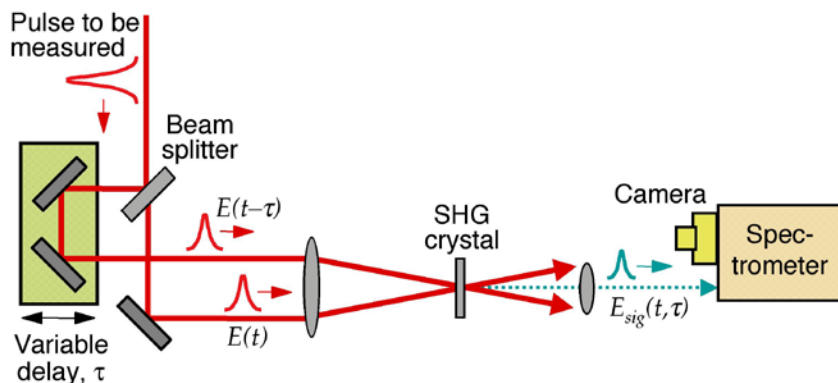


Figure 7. Schematic of a FROG (frequency-resolved autocorrelation) apparatus [6]

The FROG trace is the spectrogram of the pulse. Extracting the temporal intensity and phase from a FROG trace is equivalent to the *two-dimensional* phase-retrieval problem, which has been shown to be essentially well-posed,[7], unlike that of autocorrelation, which is a *one-dimensional* phase-retrieval problem, which is badly ill-posed and has infinitely many solutions. Simple, reliable iterative algorithms exist for finding the pulse field,  $E(t)$  from its FROG trace. [7] A few so-called “trivial ambiguities” exist, but, fortunately, they are of little interest in most pulse-measurement problems [6, 8]. In any case, for essentially all pulses, FROG works extremely well.

To retrieve pulses using FROG, we use modified phase-retrieval routines, which have proven to be very robust and fast, usually converging in  $< 0.1$  second,[6] unless the pulse is very complex. Indeed, FROG has become an effective and versatile way to measure ultrashort laser pulses, whether a 20 fs UV pulse or an oddly shaped IR pulse from a free-electron laser [6]. And FROG now routinely measures the intensity and phase of pulses from 100ps to a few fs, and variations on it are now measuring attosecond pulses [9, 10]. No other method has approached FROG’s success and versatility in measuring such a range of pulses. [11]

Finally, FROG has the convenient feature that it yields feedback confirming the measurement. Because the measured FROG trace massively over-determines the pulse (it has  $N^2$  points and there are  $2N$  unknowns), when the measured trace agrees with the retrieved trace, the measurement is very likely to have been performed correctly. If not, then the device could have been misaligned, or the input pulse may have had one or more of many spatio-temporal distortions, and the measurement should not be trusted. Because pulse measurement can be very difficult, this feedback is extremely helpful.

So, considering that we want to characterize the output of a fiber amplifier in a single shot, and that it is difficult to find a suitable reference laser to gate it with, FROG seems like the ideal choice. But so far, FROG has never been used for measuring pulses longer than  $\sim 100$ ps, and even this was very difficult [12].

One challenge in measuring pulses longer than  $\sim 100$ ps with FROG is the required spectral resolution. The second harmonic of a 3ns pulse can have spectral features as small as  $\sim 0.2$ pm, requiring far more resolution than typical diffraction-grating spectrometers have. To solve this problem, we use an etalon, which has  $\sim 100$  times more angular dispersion than a diffraction grating [13, 14]. The operation of our etalon spectrometer is described in Section 4.2. For a multi-shot measurement, FROG can be extended to the nanosecond regime by using an etalon spectrometer and a long scanning stage (a few meters long), although such a long delay stage is also challenging.

Of course, a more compact technique is vastly preferred. Also, a single-shot technique is also really necessary to sufficiently determine whether or not there is pulse-to-pulse stability in a fiber amplifier. Simply crossing two pulse replicas at an angle, which maps delay onto transverse position, the method used for single-shot fs FROGs, is not practical for such large delays. Instead, it turns out that we can *tilt* the pulse front so that one edge precedes the other by *several ns*. We discuss pulse-front tilt (PFT) in Section 5.4. Section 5.5 discusses the PFT-based single-shot ns-FROG, and in Section 5.6 we show a simplified, very elegant version of this device based on a simplified FROG technique we developed previously.

## 5.2 Etalon Spectrometer

### 5.2.1 Introduction

An etalon is simply two parallel highly reflecting surfaces, in which the output beam is the superposition of many delayed replicas of the input beam. The delay between each replica is  $2nd/c$ , where  $2d$  is the etalon round-trip length, and  $n$  is the refractive index of the medium inside the etalon. Due to the interference of the many output beams, only colors having a wavelength that is an integer ( $m$ ) multiple of the etalon's width, or  $m\lambda_0/n = 2d$ , exit the cavity without loss. Therefore, when focusing into an etalon, a range of path lengths are present, one for each ray, and so different colors will exit the cavity along different rays, or angles, resulting in its well-known angular dispersion [13]. Because etalons are usually very lossy due to the highly reflective coating required on their entrance surface, we use an etalon with a small transparent gap on its entrance surface, which reduces the loss to essentially zero, and is usually referred to as a virtual image phase array (VIPA) [14] (see Figure 8).

A previous paper showed that such an etalon generates as much as 0.8 nm/deg of angular dispersion, which is about 20 times more than what is typically achieved with a diffraction grating [14]. In fact our calculations and measurements indicate that by optimizing the parameters of the etalon and the focusing lens, much more angular dispersion can be achieved than what has previously been reported for etalon spectrometers. As much as 15deg/nm of angular dispersion can be achieved with an etalon, which makes it possible to construct an incredibly small and very high-resolution spectrometer.

We began our work to make a nanosecond-FROG by first constructing and testing VIPA etalon spectrometers for both 532nm and 1064nm. We also determined the line widths of the etalons that we purchased, which later told us the range of the FROG devices that we built out of these etalons. These results and methods are discussed below.

### 5.2.2 Testing the Etalon Spectrometer

A schematic of a VIPA etalon spectrometer is shown in Figure 8. We first bought a 5.3 mm thick, glass-spaced etalon from Precision Photonics with a window size of 20 x 12 mm. Later we bought similar etalons from CVI both for 1064nm, for measuring the spectrum of the fundamental, and for 532nm, or for measuring the second harmonic. The CVI etalons are either one inch square, or round with a 1 inch diameter with a 97% reflectivity on the front, and 99.3% at the back surface. For 532nm we acquired thicknesses of 10 and 15mm and for 1064nm thicknesses of 5 and 10mm.

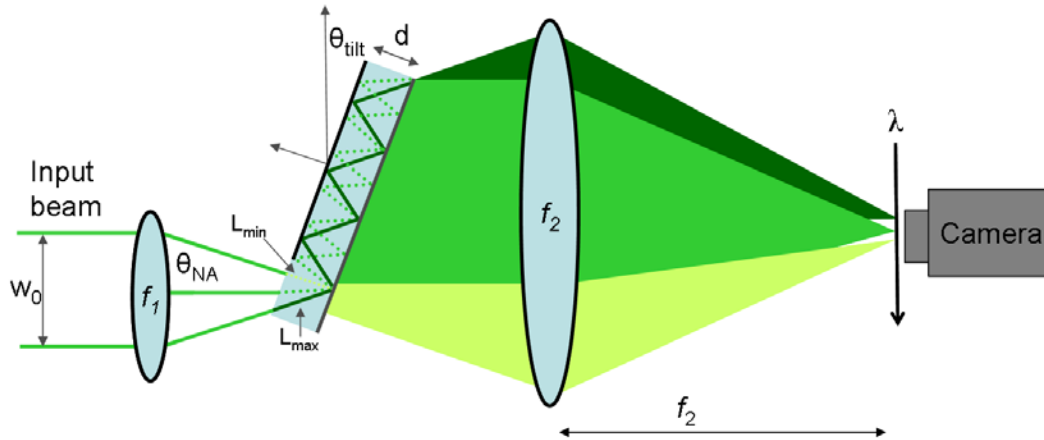


Figure 8. Etalon spectrometer

To test our etalon spectrometer at 532nm, we generated the second harmonic of the output of our 1064 nm, Standa microdisk laser. The beam to be spectrally resolved is focused into the transparent gap of the etalon using a 300 mm focal length cylindrical lens ( $f_1$ ), and the etalon tilt angle  $\theta_{\text{tilt}}$  is less than  $f$ . Different colors should exit the etalon at different angles, so as in an ordinary diffraction grating spectrometer, we use a lens to take a Fourier transform from angle to position, so that at the focal plane ( $f_2$ ), different colors are at different positions, or the camera's vertical axis will correspond to wavelength. For the second lens we also used a cylindrical lens and its focal length was  $f_2 = 200$  mm.

The parameters used for the spectrometer given above were determined from our simulations in order to maximize the angular dispersion, and these results are shown in Figure 9. According to our calculations, this geometry should result in  $\sim 15^\circ/\text{nm}$  of angular dispersion, which is enormous! Also, if the finesse is 100, then we will obtain a line width (which will also be the spectral resolution) of 0.2 pm (193 MHz).

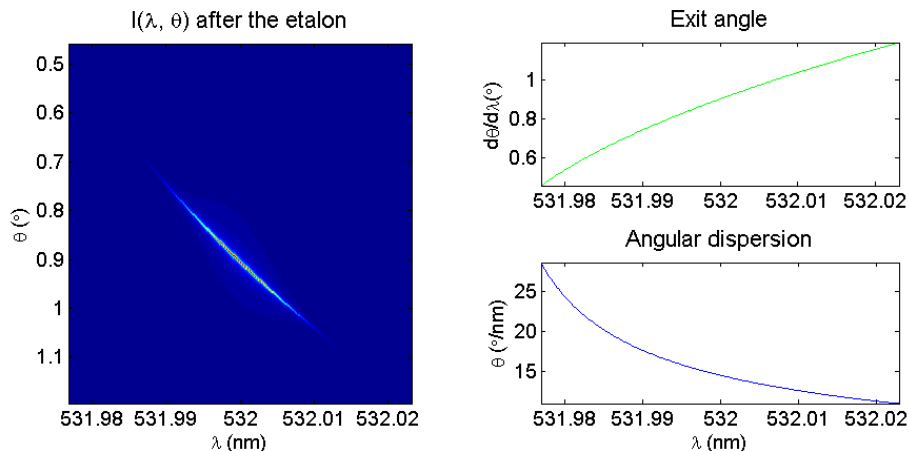


Figure 9. Simulations of the output of our etalon spectrometer

We measured the spectrum of the second harmonic of the 1064 nm microdisk laser with the etalon spectrometer. To ensure that we were measuring the spectrum, to determine the

calibration of our wavelength axis, and to see how small of a feature we could resolve, we sent the pulse through a Michelson interferometer and generated a double pulse as shown in Figure 10.

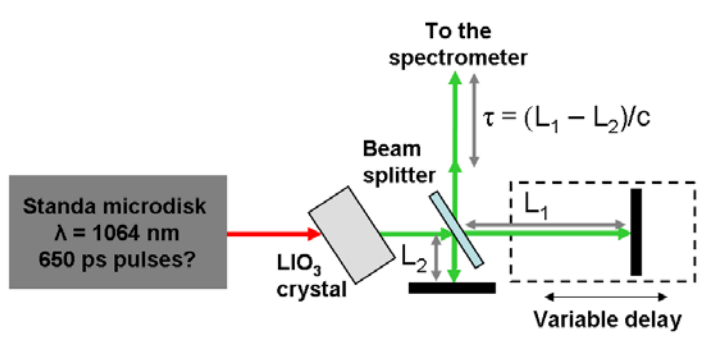


Figure 10. Experimental setup for testing and calibrating the VIPA spectrometer

Double pulses are very useful for testing the spectrometer because the spacing in time between the two pulses depends on the path length difference  $\Delta L = L_1 - L_2$ , and such a pulse has fringes in its spectrum with a spacing of  $\lambda^2/(2\pi \Delta L)$ . Therefore we can generate fringes in the spectrum and calculate the spacing between these from the introduced path length difference.

Figure 11 shows several different spectra that we measured using the experimental setup shown in Figure 10. The spectra in Figure 11, which have fringes, were generated at three different positions of the variable delay stage. The three  $\Delta L$ 's of 64, 40 and 19 cm correspond to fringe spacings of 0.07, 0.11 and 0.22 pm respectively. These spectral fringes nicely demonstrate that we are indeed measuring the spectrum, and we can see fringes with a calculated spacing of only 0.07 pm. We use such measurements to determine the calibration or number of picometers per pixel.

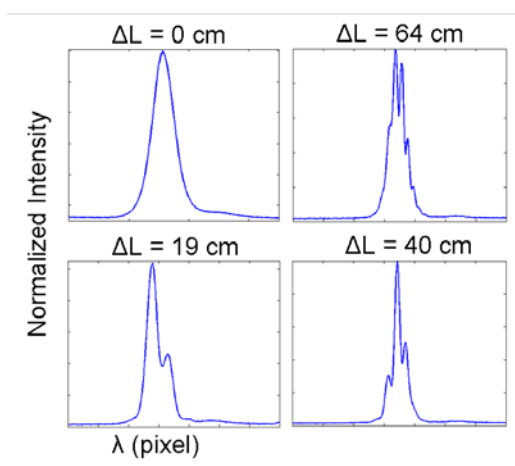


Figure 11: Spectra measured with the etalon spectrometer

### 5.2.3 Measuring the Free Spectral Range of the VIPA etalons

Using the spectral fringes generated by the Michelson interferometer, we can quantify the spectral resolution of the 532nm etalon spectrometer, or equivalently the line width of the 1cm

etalon. Knowing this allowed us to quantify the measurement range of the FROG that we later built. It is also useful to know this because it could be deconvolved from the measured FROG traces to improve the retrieved results.

Finite spectral resolution, which can be viewed as a convolution of the ideal spectrum with a spectral response function, smears out smaller spectral features more. By measuring the spectral fringe contrast in the double pulse spectrum as we decrease their spacing, we can determine the spectral response function of our etalon spectrometer [15-18]. This idea is illustrated in Figure 12.

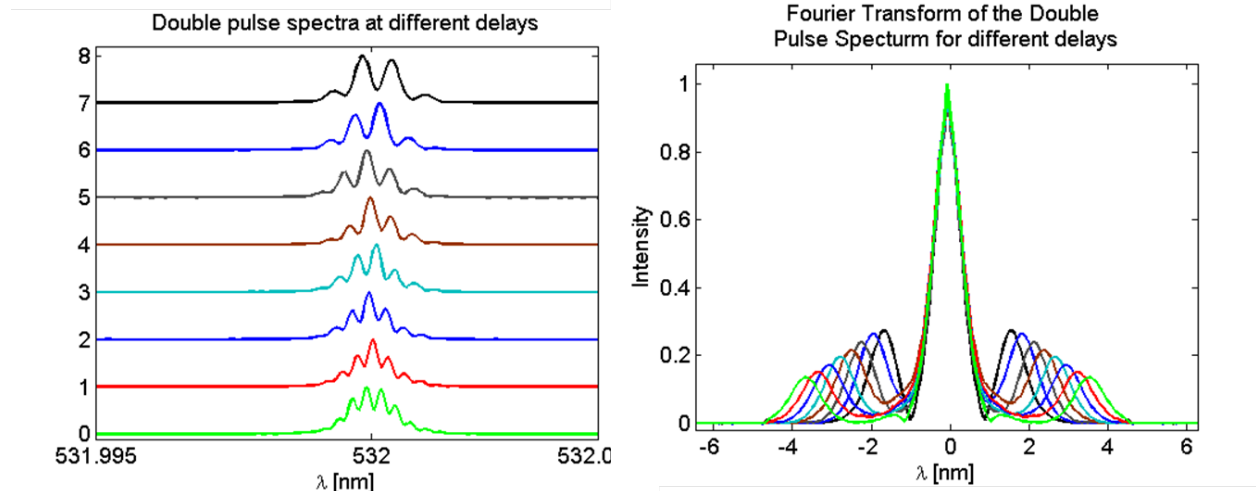


Figure 12. Measuring the spectral response function of our 532nm etalon spectrometer

The plot at the right of Figure 12 shows the spectrum from the central lobe of the FROG traces as we decreased the double pulse spacing from about 1.8ns to 4ns. It is apparent that the slower fringes are better resolved or have a better contrast. To quantitatively extract the contrast, we Fourier transform each spectrum to the time domain, which results in 3 peaks. The fringe contrast is the relative height of the side bands to the central peak, which would be 0.5 in the ideal case and the same for every spectrum. But it is evident that the sidebands are weaker for the spectra with faster fringes. Because finite resolution is a convolution in the frequency domain, it is a product in the time domain. Therefore, we can read off the peak height of the sidebands at each time to construct the so-called temporal response function, which is shown in Figure 13 (left).

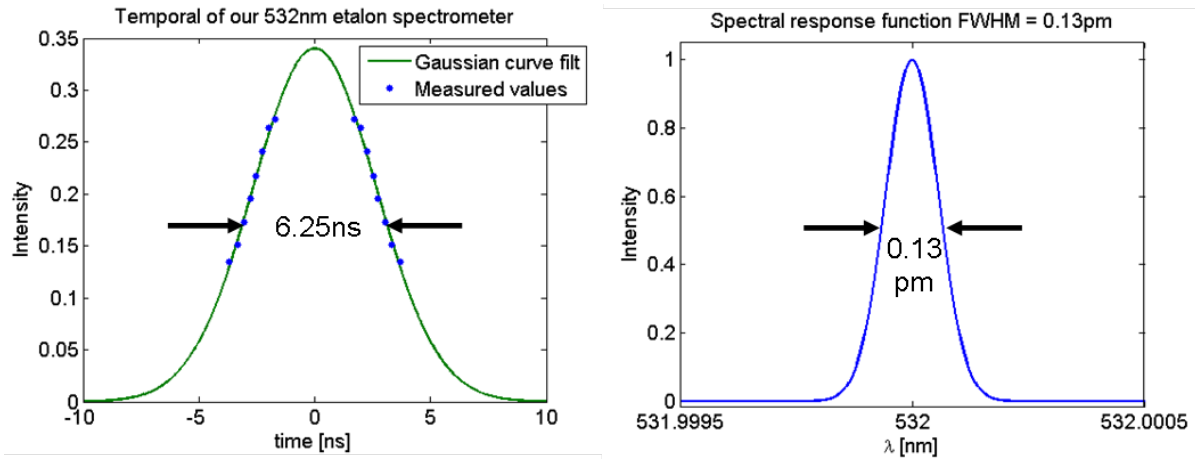


Figure 13. Temporal response (left) and spectral response (right) of our 1cm thick 532nm etalon

The spectral response function can then be obtained by Fourier transforming this, and the spectral resolution is the FWHM of this function. Assuming that this function is symmetric, we performed a curve fit and found it to be very similar to a Gaussian. The Fourier transform, or the spectral response function, is shown at the right and it has a FWHM of 0.13pm (138 MHz).

To determine the line widths of the two 1064nm etalons, we used a wavelength-tunable (1030-1070nm) New Focus Velocity laser. This laser has a line width about 1000 times narrower than what we expect for the etalons ( $<1\text{MHz}$ ,  $<1\text{fm}$ ), and therefore measuring its spectrum with our etalon spectrometer directly tells us the spectral response function or line shape of the etalons. To calibrate the spectrometer, we can also scan the wavelength of the cw laser by a known amount and see the number of pixels that the spectrum moves. The results of our measurements for the 5mm and the 10mm wide 1064nm etalons are shown in Figure 14 and Figure 15.

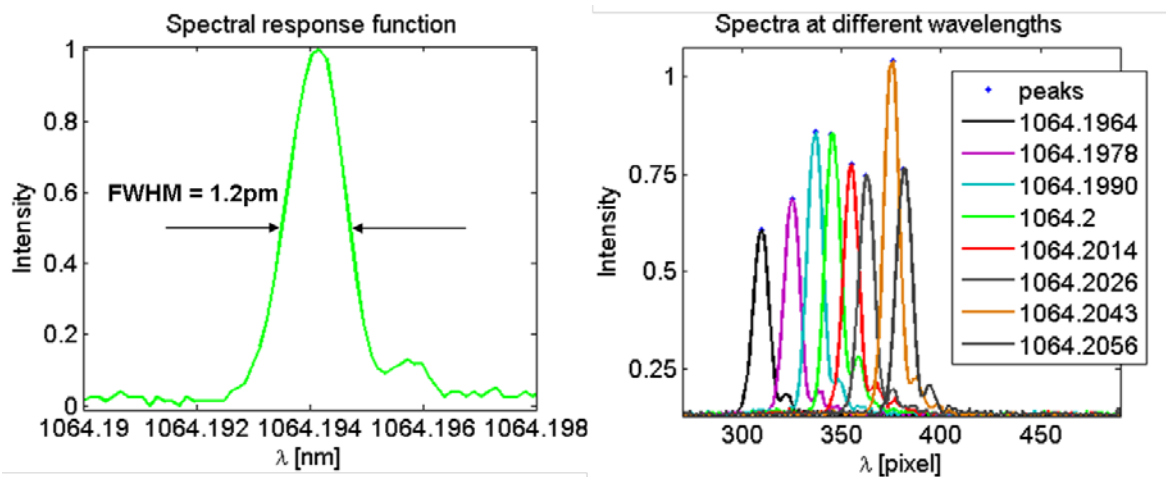


Figure 14. Measuring the line width of the 5mm, 1064nm VIPA etalon

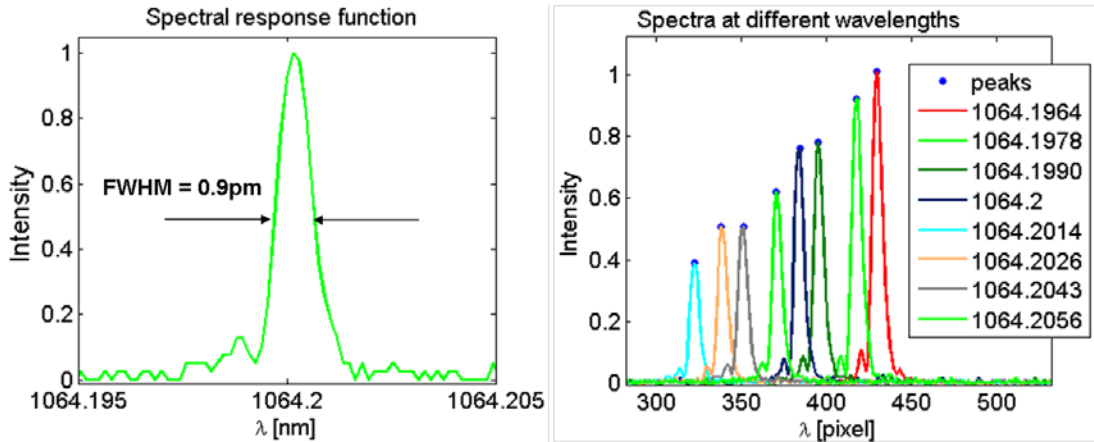


Figure 15. Measuring the line width of the 1cm, 1064nm VIPA etalon

These plots confirm the relevant features of these etalons—that their line widths are narrow and that the angle of the beam emitted from them depends on the beam’s wavelength. Note that, in each case (the right plots of both figures), the peak of the detected curve moves by an amount directly proportional to the wavelength involved. We found the etalon-spectrometer line widths to be 0.9pm (240MHz) and 1.2pm (320MHz) for the 5mm and 1cm etalons respectively.

### 5.3 Multi-Shot ns-FROG

Once we were able to measure the spectrum of 1064 nm, ~700 ps pulses from the Standa Laser, as described in the previous section, it is straightforward (if inconvenient) to make multi-shot FROG measurements of these pulses. Our multi-shot ns-FROG is very similar to what was described in section 5.1; we just need a longer delay stage and the etalon spectrometer. To make the FROG measurement, we split the pulse into two, recombine the beams in a second harmonic crystal with a delay between them, and then measure the spectrum of second harmonic signal generated at each delay. A schematic of this is shown in Figure 16.

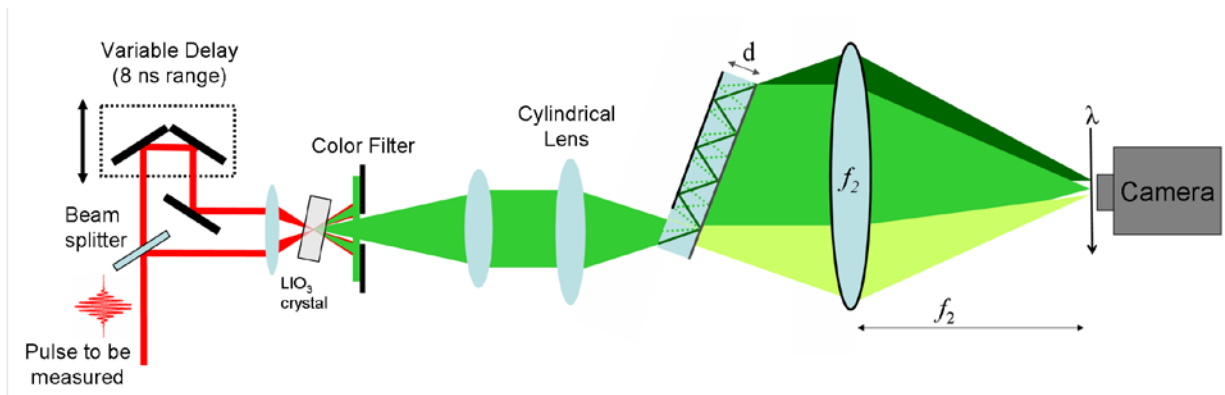


Figure 16. Schematic of our multi-shot FROG

Specifically, our multi-shot FROG uses a 3mm thick  $\text{LiO}_3$  crystal as the nonlinear medium, which we focus into with a 20 cm spherical lens. The delay stage has a range of 60 cm, or 2 ns, which we double pass using two corner cubes so that our total delay range is 8 ns. In the

spectrometer, we used the 5mm precision photonics etalon, because at the time, we had not yet received the higher resolution CVI etalons.

For our first measurements, we made a FROG trace of the seed laser pulse. This FROG trace is the top right image in Figure 17.

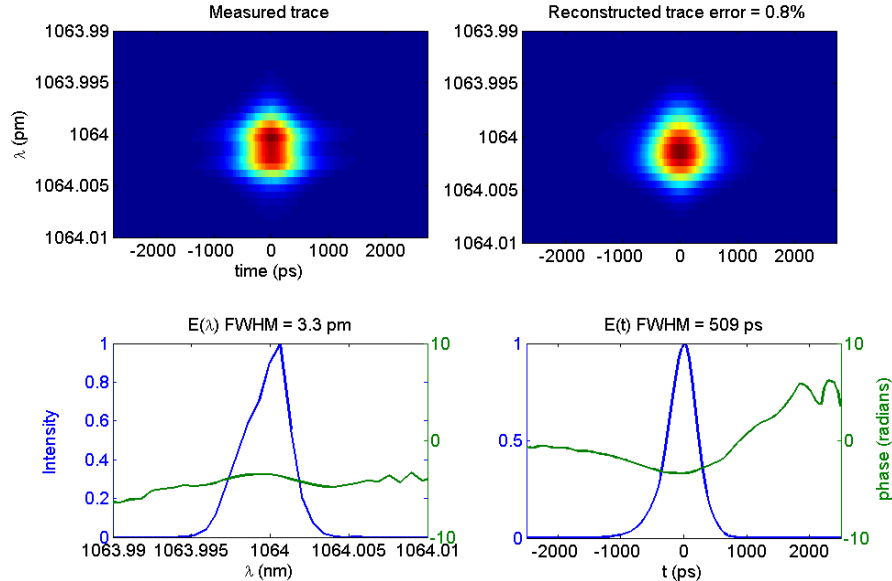


Figure 17. FROG measurement and retrieval results of the pulses from the Standa microchip laser

To obtain the complete electric field of the pulse from the FROG trace, we use the generalized projections algorithm, which is described in detail in reference [1]. Briefly, because it is not possible to directly invert the FROG trace to obtain the intensity and phase of the pulse, we use an iterative algorithm. This algorithm begins with an initial guess of the pulse’s intensity and phase (usually random noise), which it modifies until the FROG trace constructed with this guess is as close as possible to the measured one. When the RMS difference between the measured and so-called retrieved traces is less than 1-2 % (sometimes called the FROG error, or retrieval error) we say that the algorithm has converged. At this point, the modified guess is the intensity and phase of the pulse that was measured.

The reconstructed FROG trace for our measurement is shown at the top right of Figure 17, and the retrieval error was 0.8 %. The intensity and phase of the pulse are shown at the bottom of the figure in both the frequency and the time domains. It is evident that the pulse bandwidth is 3.3 pm, and its duration is 509 ps. The quadratic phases indicate that the pulse has a little negative chirp. A pulse with 3.3 pm of bandwidth has a transform-limited pulse duration of 488 ps.

Later, after doing the careful analysis of the line shapes of all of our etalons (see section 4.2.2), we realized that, due to the low resolution of the Precision Photonics etalon, the measured spectrum was broadened in this measurement. This made the pulse that we measured appear to be a little shorter than it really was. Our measurements in section 4.4 and 4.5 using the CVI etalons show a pulse duration of 720ps, which is closer to the company’s promised value of 670ps.

To further test our FROG device, so that we can have complete confidence in what it measures, we again made a double pulse with the Michelson and measured this pulse. The double pulse is a good test because we know what its pulses shape in time is: two pulses with a delay between them equal to  $\Delta L/c$  where  $\Delta L$  is the path length difference. The path length difference in our Michelson was 53.2 cm which should result in a 1.76 ns double pulse separation. We can also check the relative height of the pulses from the Michelson using a power meter, which we found to be 0.9. The results of this FROG measurement are shown in Figure 18.

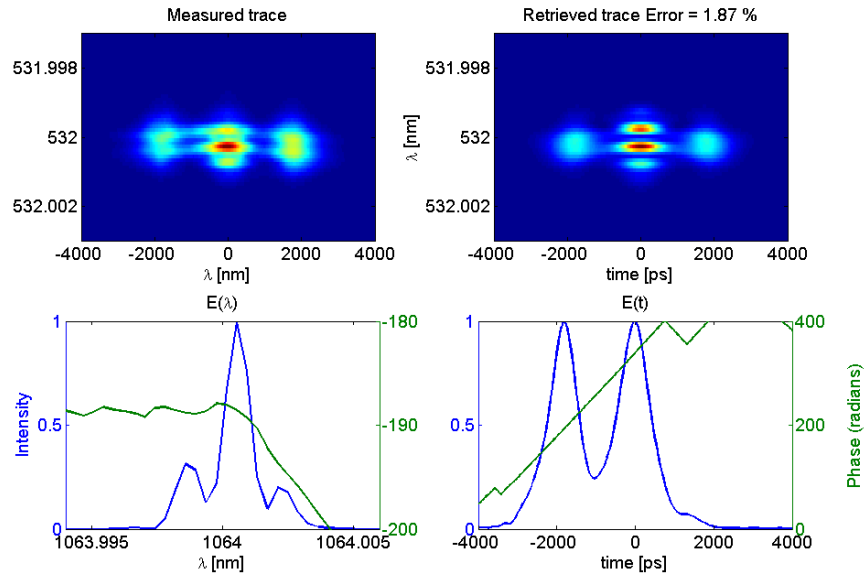


Figure 18. FROG measurement and retrieval results for a 1.77 ns double pulse

For this trace, the FROG retrieval error is a little higher at 1.87%, and the main discrepancy between the two traces is the spectral fringe contrast. Actually, it seems that these 0.5 pm spectral fringes are already close to the resolution limit of our etalon spectrometer, and the FROG retrieval program is seeing through this (a sort of spectral super-resolution), and still retrieving close to the right answer. The relative heights of the peaks in the retrieval is 1, which is close to the expected value of 0.9, and the spacing of these peaks is correct (1.7 ns), as well as the width of the spectrum, and the spectral fringe spacing.

A FROG trace is well known to have redundant information or to over-determine the pulse, because there are  $N^2$  points in the trace, and only  $2N$  unknowns [6](the intensity and phase in either the frequency or the time domain). Another way to say this is that the delay dimension and the frequency dimension of the trace contain some of the same information. Specifically in this case, this redundant information is the relative height of the pulses in the double pulse. The relative height of the pulses is encoded in the spectral fringe contrast (or depth), as well as in the relative height of the lobes or peaks on the temporal axis. For the delay dimension, if the pulses have equal intensity, the relative height of the peaks should be  $\frac{1}{2}$  which is very close to our measured FROG trace. For the frequency axis, equally intense peaks result in a spectral fringe contrast of 1, or the intensity between the fringes should go to zero. This is not the case for our measured FROG trace due to the smearing that happens when working close the limit of a

spectrometer’s resolution. But because the information is correct along the delay axis, and only slightly distorted along frequency axis, the FROG retrieval algorithm returns a trace with better spectral fringe contrast, which is likely the trace that we would have measured if we had had better spectral resolution. And indeed the retrieved pulse shape is very close to what we expect.

## 5.4 Nanosecond Pulse-Front Tilt (PFT)

In the previous section we demonstrated a multi-shot nanosecond-FROG, though our ultimate goal is to develop a *single-shot* method. To do this we needed a way to map delay onto position with nanoseconds of range. We realized that the same etalons that we were using to make a high resolution spectrometer could also generate a massively tilted pulse front, and that this 89.95 degree tilted pulse front could be used to generate our nanosecond delay range. Before discussing the FROG that we built based on this idea, we explain here how this nanosecond tilted pulse front comes about. We also made interferometric measurements to verify that we were generating nanoseconds of pulse front tilt and quantify it.

### 5.4.1. Introduction

It is well known that the temporal and spatial dependencies of the electric field of pulsed radiation are often coupled and cannot be assumed to be independent, especially for femtosecond pulses [19]. This is because common optical elements, can introduce *spatiotemporal couplings* or cross dependencies in  $x$  and  $t$  in the light pulse’s electric field. The most common spatiotemporal coupling is *angular dispersion* which is introduced by many optical elements, such as prisms, diffraction gratings, and etalons as shown in the previous section.

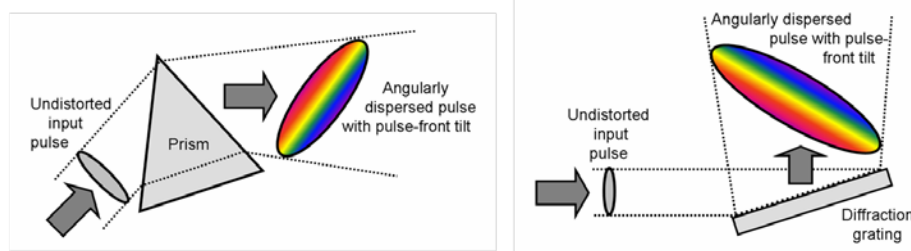


Figure 19. Prisms and diffraction gratings introduce angular dispersion, or, if viewed in time, pulse front tilt

Because the electric field  $E(x,t)$  of the pulse can be represented equivalently in any Fourier domain,  $xt$ ,  $x\omega$ ,  $k_x\omega$  or  $k_x t$ , a given spatiotemporal coupling actually manifests itself as several seemingly different, but equivalent, effects when viewed in any of the other domains[19]. So, while angular dispersion is an intensity cross term in the field  $E(k_x,\omega)$ ,

$$\hat{\tilde{E}}(k_x, \omega) = \hat{\tilde{E}}_0[k_x + \gamma(\omega - \omega_0), \omega] \quad (3)$$

where  $\gamma$  is the coupling constant and  $\omega_0$  is the pulse center frequency, simply Fourier transforming to the  $xt$  domain (and applying the shift and inverse shift theorems), it is easy to see that there is always a corresponding  $xt$  coupling in the intensity known as *pulse front tilt* [20-22]:

$$E(x,t) \propto E_0(x,t + \gamma x) \quad (4)$$

In the absence of spatial or temporal chirp, the pulse-front tilt is linearly proportional to the angular dispersion—independent of the cause of the angular dispersion—so, because diffraction gratings generally introduce more angular dispersion than prisms, they also yield a more tilted pulse front. While the pulse-front tilt from diffraction gratings and prisms has been investigated in detail, Bor, *et al.*, have pointed out that less commonly used sources of dispersion, such as etalons [21], also introduce pulse-front tilt. And because their angular dispersion can be orders of magnitude more than that of prisms and gratings, their pulse-front tilt can be extremely large.

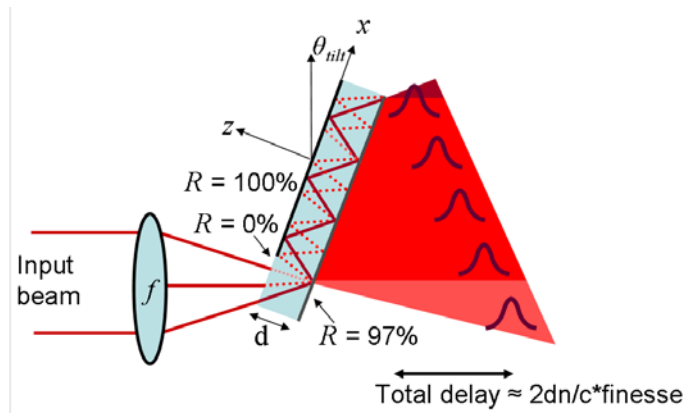


Figure 20. Schematic of the tilted pulse front that emerges from a “VIPA” etalon

The huge angular dispersion of etalons implies that their output pulse front must be very tilted—by as much as 100 times that due to a diffraction grating. That can be seen by simple light-travel-time considerations: the part of the pulse that makes the most passes through the etalon sees the most delay. And the thicker and more reflective the etalon, the more the dispersion and tilt.

To test this, we simulated and measured the complete spatiotemporal field of a 500ps, 3pm bandwidth pulse sent through an etalon. For the simulations, we simply superimpose delayed and successively defocused replicas of the input pulse, where the number of replicas is chosen to produce the correct line width. Measuring the output pulse in space and time from the VIPA etalon is considerably more challenging. And considering that diffraction gratings typically produce a maximum of 3ps/mm of pulse front tilt (the grating size times the speed of light, see Figure 20), the VIPA etalon can be expected to produce several *nanoseconds* of pulse front tilt across a 1cm beam, due to its increased angular dispersion, corresponding to a massively tilted pulse.

We measure the spatio-spectral phase added to the pulse by the etalon in a linear interferometric frequency-domain technique used for measuring femtosecond and picosecond pulses, but extended to the nanosecond regime. We use the variation of spectral interferometry [23] usually known as crossed-beam spectral interferometry, which literally involves measuring a spectrally resolved spatial interferogram [24-27]. This requires a spectrometer with spectral resolution equal to the inverse of the unknown pulse duration, or for our case <1pm. For this we used a VIPA etalon spectrometer. As a reference pulse we use the beam directly from the laser, which is crossed with the tilted pulse out of the etalon at a small angle at a camera to produce spatial interference fringes. In the other dimension, we spectrally resolve the interference fringes using a VIPA-etalon spectrometer so that a two-dimensional interferogram  $I(x,\lambda)$  is measured. Using Fourier filtering along the  $x$ -dimension, the field of the tilted pulse's field  $E_{\text{unk}}(x, \lambda)$  is determined [26].

#### 5.4.2. Modeling the Spatiotemporal Field of the Pulse From a VIPA Etalon

Intuitively we can estimate the pulse front tilt by considering that each delayed replica is also spatially shifted along the  $x$  direction due to the etalon's tilt angle  $\theta_{\text{tilt}}$  (see Figure 20). So we expect the left side of the beam to be ahead in time compared to the right side by approximately  $2dn/(c \cos\theta_{\text{tilt}})$  multiplied by the number of bounces of the beam inside of the etalon. Considering that the number of bounces is approximately given by the finesse,  $\mathcal{F}$ , which we found experimentally to be 50 (see section 3), for  $d = 5\text{mm}$ ,  $n = 1.5$ , and with  $\theta_{\text{tilt}} = 1^\circ$ , this results in 2.5ns of pulse front tilt, across an output beam with a width along the  $x$  dimension of  $\sim 5.8\text{mm}$ .

To more precisely calculate the field emerging from the VIPA etalon shown in Figure 20, for a given input pulse that is free of spatiotemporal couplings as well as temporal chirp, we simply superimpose the emerging delayed, diverging, transversely displaced replicas.

We start with the field just after the lens  $E_{\text{in}}(x,\lambda)$ , which is given by:

$$E_{\text{in}}(x, \omega, z = 0) = \exp\left(-\frac{(\omega - \omega_0)^2}{\Delta\omega} - \frac{(x)^2}{w_0} - ikx \sin \theta_{\text{tilt}} + i\frac{k_0 x^2}{2f}\right), \quad (5)$$

where  $\theta_{\text{tilt}}$  is the incident angle of the center ray at the etalon,  $w_0$  is the input beam spot size, and  $\Delta\omega$  is the spectral bandwidth. See Figure 20 for the other parameters. The field immediately after the etalon is given by:

$$E_{\text{out}}(x, \omega) = t_1 t_2 \sum_{m=0}^{\mathcal{F}} (r_1 r_2)^m E_f(x, \omega, 2dm). \quad (6)$$

where  $t_1$ ,  $r_1$ ,  $t_2$  and  $r_2$  are the reflection and transmission coefficients of the 1<sup>st</sup> and 2<sup>nd</sup> surfaces of the etalon, and  $E_f = E_{\text{in}}(x, \omega, z = f)$ , that is, the field at the focus. To calculate the spatio-spectral field after each pass through the etalon, we use the angular spectrum of plane waves approach [28], to propagate the field from the previous pass, by an additional distance of  $2d$ , as shown below:

$$E_f(x, \omega, 2dm) = \mathfrak{F}_x^{-1} \left\{ \mathfrak{F}_x \left\{ E_f(x, \omega, 2d(m-1)) \right\} \exp\left(i2dnk_0 \sqrt{1 - (k_x \lambda)^2}\right) \right\}. \quad (7)$$

This involves a one-dimensional Fourier transform of the initial field to the  $kx$ -domain, multiplying this field by the propagation kernel as a function of  $kx$ , and then inverse Fourier transforming back the  $x$ -domain. The same approach is used to propagate the initial field  $E_{in}(x,\omega)$  up to the etalon's front surface to generate  $E_f(x,\omega)$ . The results of these simulations using our experimental parameters are shown in the next section.

Previous authors have described a similar approach for modeling VIPA etalons, but they instead derived an analytical expression for the field at the focal plane of a lens placed after the etalon, which is used for making a VIPA etalon spectrometer [29].

#### 5.4.3. Measuring the Spatiotemporal Field of the Pulse From a VIPA Etalon

We used crossed-beam spectral interferometry to measure the spatiotemporal intensity and phase added to the input pulse by a VIPA etalon (referred to as the PFT etalon) like that shown in Figure 20. The back surface of the etalon is imaged onto a camera in the  $x$ , or angular dispersion dimension of the PFT etalon, and in the other dimension, it is spectrally resolved with a 2<sup>nd</sup> VIPA etalon spectrometer to achieve the needed spectral resolution. A spatially clean reference pulse crosses at a small angle with the tilted or unknown pulse to produce the following interferogram at the camera:

$$I(x, \lambda) = |E_{ref}(\lambda)|^2 + |E_{unk}(x, \lambda)|^2 + 2|E_{unk}(x, \lambda)E_{ref}(\lambda)|\cos(kx\theta_c + \varphi_{unk}(x, \lambda) - \varphi_{ref}(\lambda)), \quad (8)$$

where  $\theta_c$  is the crossing angle between the beams. The interferogram that we measure is the same as that measured in a simplified version of spectral interferometry we recently developed [25], except that the spatial information of the unknown pulse is measured, because no fibers are used in our setup. Therefore we use an identical Fourier filtering procedure to that used for this simplified technique to extract the spatio-spectral intensity and phase of the unknown pulse from the measured interferogram [25, 26]. This process is illustrated in Figure 21. Retrieving the spatio-spectral field of the unknown pulse from the interferogram.

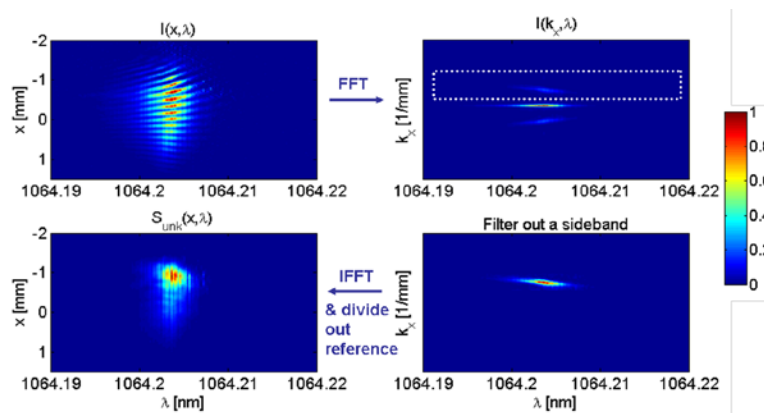


Figure 21. Retrieving the spatio-spectral field of the unknown pulse from the interferogram

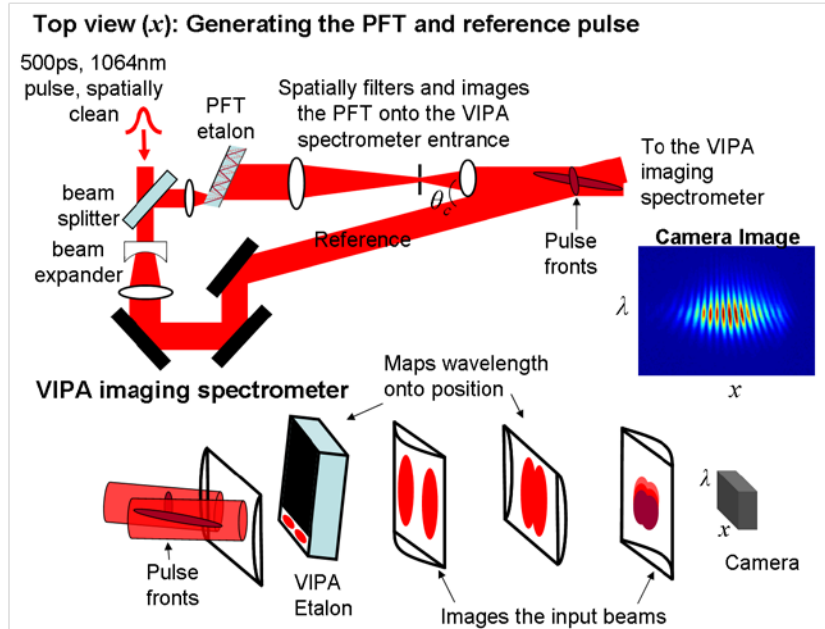


Figure 22. Experimental setup for measuring the spatiotemporal field of the pulse from an etalon

The top right image in Figure 22 shows a typical interferogram that we measured. The fringes along the  $x$ -dimension are due to the beams' small crossing angle. That their periodicity varies with wavelength is due to the angular dispersion in the beam from the etalon. Similarly, for larger values of  $|x|$ , there are some spectral fringes due to a delay between the reference and unknown pulses due to the tilt of the unknown pulse front. To measure the interferogram described above in order to characterize the tilted pulse out of an etalon, we use the experimental setup shown in Figure 22.

As our source we used a Standa Nd:LSB microdisk seed laser laser. To study the pulse after the VIPA etalon, we put a beam splitter at the output of the laser forming a reference and unknown arm of the interferometer. The unknown beam passes through the 1<sup>st</sup> VIPA etalon (called the PFT etalon and with  $d = 5\text{mm}$  and from CVD), adding PFT. The pulse from the etalon propagates through a spatial filter, which removes the higher orders from the PFT etalon. This also demagnifies the beam by  $2\times$  and images it onto the entrance of the VIPA imaging spectrometer. Here the reference beam crosses at a small angle and spatially overlaps with the unknown beam. The VIPA imaging spectrometer images the crossing beams onto the camera's  $x$ -dimension resulting in spatial interference fringes. Along the camera's other dimension, the crossing beams are spectrally resolved using a second, wider etalon ( $d = 10\text{mm}$ ) to generate angular dispersion, and then a cylindrical lens to map angle, or color onto position at the camera. This results in a two-dimensional interferogram at the camera. Note that, for flexibility, two lenses are used in the imaging spectrometer in order to achieve the desired demagnification of  $2\times$ .

In the experimental setup shown in Figure 22, the cylindrical lenses used to focus into the etalons both had focal lengths of  $100\text{mm}$ , and the lens in the spectrometer had a focal length of  $500\text{mm}$ . We estimated the etalon tilt angle with respect to the beam,  $\theta_{tilt}$ , to be around  $1^\circ$ , and we found a

value of  $0.9^\circ$  to produce simulations that fit best with what we measured. There was a total demagnification of  $4\times$  of the beams at the camera:  $2\times$  from the spatial filter, and  $2\times$  from the imaging lenses in the spectrometer. It is important to image the output of the etalon onto the camera, because, as the pulse containing angular dispersion propagates, spatial chirp is generated reducing the pulse-front tilt due to the decreased local bandwidth [21].

Note that in the above setup, and using the retrieval described in the previous section, we measure the spatio-spectrum and intensity added to the unknown pulse by the 1<sup>st</sup> etalon. Any phase terms that the unknown and reference pulses have in common, such as chirp in the laser output, cancel out in this measurement.

#### 5.4.4 Results and Discussion

Using the experimental setup described above, we measured the spatio-spectral field  $E(x,\lambda)$  of the pulse just after the etalon. Because we know the spectral line shape of the etalon in the spectrometer, we first deconvolved this from the measured interferograms using MATLAB's built-in Richardson-Lucy algorithm. Then we retrieved the unknown pulse using the Fourier filtering algorithm described above. We Fourier transformed the retrieved field to both the  $k_x x$  and  $x t$  domains to see the angular dispersion and the pulse-front tilt. The experimentally retrieved intensities in these three domains are shown at the top of Figure 23.

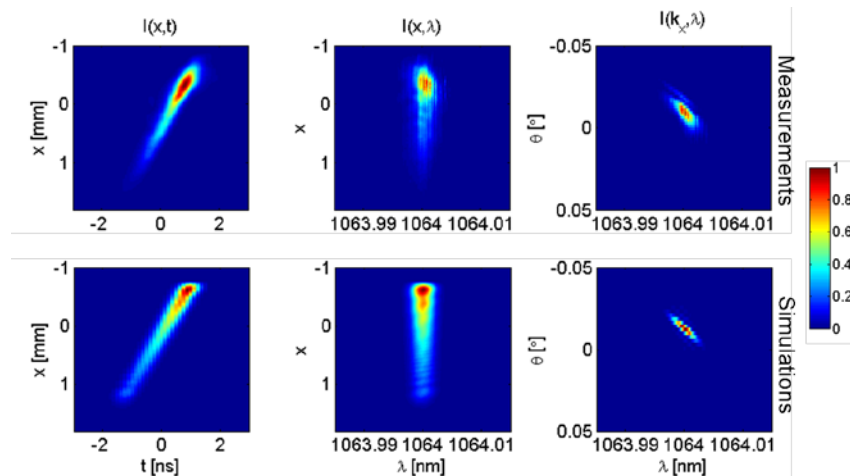


Figure 23. Measurement (top) and simulation (bottom) of the spatiotemporal field after a VIPA etalon

We also performed simulations using all of the experimental parameter and the method described in the previous section. These results are shown at the bottom of Figure 23.

As expected, the intensity  $I(k_x,\lambda)$  shows a tilt, indicating that different colors are propagating at different angles (where  $k_x=2\pi/\lambda\cos\theta$ ) due to the angular dispersion introduced by the etalon. By finding the maximum in the spectrum for each angle, we found the tilt to be linear and have a slope of  $3^\circ/\text{nm}$ . A diffraction grating with 1000 grooves/mm, used at grazing incidence and for a wavelength 1064nm results in an angular dispersion of  $0.06^\circ/\text{nm}$ , or about 50 times less than the PFT etalon. We also characterized the pulse's couplings with dimensionless  $\rho$ -parameters, which are the normalized cross moments of the pulse's two-dimensional intensity, whose magnitudes

are always  $\leq 1$  [30]. For the case of angular dispersion, we find that  $\rho_{k\lambda} = 0.015$  for the pulse from the etalon, which is quite small, due to the small bandwidth of our laser.

If angular dispersion is present, so is pulse-front tilt. This is apparent from the large tilt in the intensity  $I(x,t)$ , at the left in Figure 23. Again, curve fitting to this, we found the tilt to be linear and have a slope 1.3ns/mm, or  $\rho_{xt} = 0.27$ . The pulse out of the etalon is extremely tilted with the arrival time varying by 2.6ns, or 78cm, across the  $\sim 2$ mm beam at the camera. As mentioned above, we used  $4\times$  demagnification in the spatial filter and also in the simulations, so just after the etalon, the tilt would have been 325ps/mm.

The spatospectrum  $I(x,\lambda)$  shows no detectable tilt, and therefore no spatial chirp. The  $\rho$  parameter for this spectrum was  $\rho_{x\lambda} = 0.006$ , which is generally considered to be out of the detectable range, or just due to noise in the data [30]. In the  $x\lambda$ -domain, the coupling introduced by the etalon is known as *wave-front-tilt dispersion* [19], which is a phase coupling, which is why it does not appear in our measurements. A single Fourier transform moves a purely imaginary quantity into the intensity, which is why the coupling is apparent in the  $k_x x$ , and  $xt$  intensities as shown in Figure 23.

The agreement between our simulations and measurements is good, with the main discrepancy being in our measured spatial profile. According to our simulations, the beam's spatial profile should approximately exponentially decay along the  $x$ -dimension because, with each successive bounce in the etalon, the intensity is reduced by a factor of  $r_1 r_2$ . The spatial resolution in our measurements is limited by our ability to image the input beams through the VIPA etalon. This requires a large depth of field because each successive beam out of the etalon travels an additional distance of  $2dn$ . Therefore, the depth of field needed is  $2dn$  times the finesse, which is the propagation distance between the first and last passes of the etalon, or  $\sim 60$ cm for our 10mm etalon. Our imaging system consisted of a 30cm followed by a 15cm focal length cylindrical lens. Setting the depth of field equal to 60cm, we find that the smallest possible feature that we can resolve at the camera to be around 0.3mm. Therefore the sharp edge of the spatiotemporal profile is smeared out in our measurements.

The other discrepancy is in the width of the measured intensity  $I(k_x, \lambda)$ , which is likely due to the finite resolution of the etalon spectrometer. Even though we attempted to deconvolve its line shape from the measurements, its finite resolution cannot be accounted for perfectly in doing this. For example, the spectrometer's alignment may have been slightly different for our measurements than it was when we characterized the line width using a narrowband laser, perhaps due to the slight angle of the crossing beams.

## 5.5 Single-Shot ns-FROG

### 5.5.1 Experimental setup

Now that we have demonstrated that nanoseconds of pulse front tilt can be generated from an etalon, we can use this to make the needed delay range for a single-shot ns-FROG. A schematic of the single-shot FROG is shown in Figure 24. We use two tilted pulse fronts by placing the beam splitter after the PFT etalon. This generates two pulse replicas with tilted pulse fronts. In addition, by bouncing one replica off three mirrors and the other off two, the two pulses have

opposite tilt. By crossing two such oppositely tilted pulses, we can generate a delay range twice as large as in our previous set up.

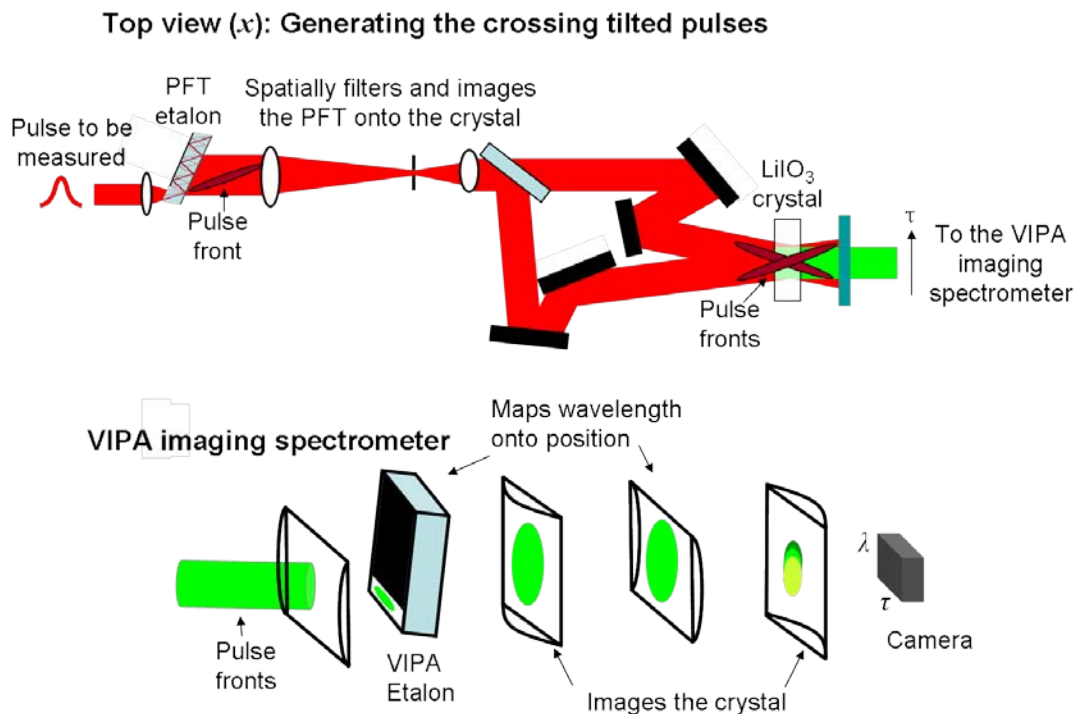


Figure 24. Our 1<sup>st</sup> version of the single-shot ns-FROG

Another nice feature of this set up results from the exponential spatial profile produced by the PFT etalon. When the two beams cross in the SHG crystal to generate the second harmonic with the delay between the two beams varying with transverse spatial position in order to make a single-shot autocorrelation, it is important that the transverse spatial profile of the beam not affect the measurement. This is because the beam that emerges is actually the autocorrelation times the product of the spatial amplitudes of the two pulse replicas. To avoid distortions due to the beams' spatial profile, it is generally believed that a spatially flat profile is required. But that is not possible here—an *exponential* transverse profile necessarily emerges from the etalon. The concern is therefore that such a variation in the beam's intensity along the horizontal transverse dimension ( $x$ ) can distort the shape of the single-shot autocorrelation. Fortunately, because the beams are inverted relative to each other, the product of their spatial amplitudes is always equal to a constant:

$$\exp(ax + b) \times \exp(-ax + c) = \exp(b + c) = \text{constant} \quad (9)$$

independently of the transverse coordinate,  $x$ , and so yielding a perfect autocorrelation, unaffected by the exponential spatial profile!

### 5.5.2 Testing the FROG

To test the FROG, we again used the double pulse from a Michelson interferometer, which yields a FROG trace unlikely to occur by chance. The measured results for a 3ns pulse separation and having a relative peak height of 60% are shown in Figure 25.

The top right image shows the FROG trace that we measured. Next we use the FROG reconstruction algorithm to extract the temporal and spectral intensities and phases from the FROG trace. The reconstructed FROG trace's similarity is a measure of convergence, and also a measure of how good a measurement is. The reconstructed and measured FROG traces shown in Figure 25 are in good agreement with a 1.4% rms difference between them. The temporal peak spacing is 3ns as it should be, and the relative height of the peaks is only slightly off, at 50% rather than 60%. The spectral fringes are spaced by 1pm. The minor discrepancies are in the spectral fringe contrast due to our imperfect spectral resolution. But note that this double pulse trace is considerably better than our previous measurements with the multi-shot FROG. This is mainly because the CVI etalon that we are now using for the 532nm spectrometer has better spectral resolution than the ones that we obtained from Precision Photonics.

We also use the double pulse trace to calibrate the delay and frequencies axes because we know where the peaks should be given the path length difference of our Michelson interferometer. So now that the FROG is successfully calibrated, we used it to measure the output of the Standa seed laser, which is shown below.

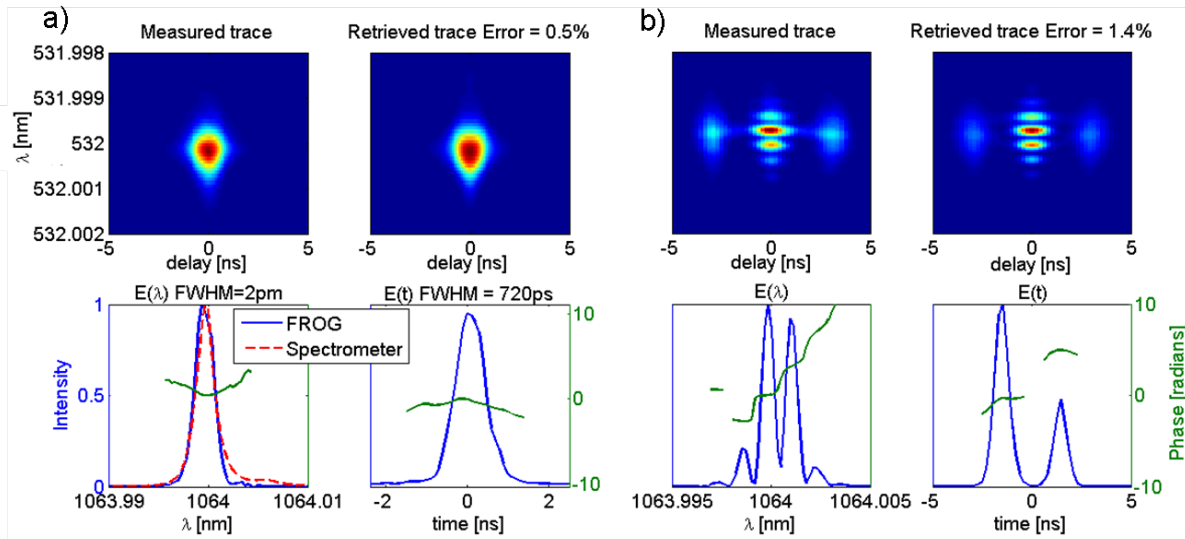


Figure 25. FROG measurement of the seed laser (a) and a 3ns double pulse (b)

The measured and retrieved traces are in very good agreement, and the resulting temporal and spectral fields are shown below the traces. We found the pulse from the seed laser to be 720ps long with a 2pm bandwidth. This is not in agreement with the results we obtained previously when using the multi-shot FROG and the precision photonics 532 etalon, which were 3pm, 510ps. This is mostly likely because the 532nm Precision Photonics etalon had poorer spectral resolution than the CVI etalons. We estimate that the Precision Photonics etalon spectral resolution was  $\sim 1\text{pm}$  which would significantly broaden the second-harmonic spectrum, while

the CVI etalon resolution is probably more like 0.2pm. Therefore the broadened spectrum measured with the Precision Photonics etalon likely made the pulse appear to be shorter. So the results shown in Figure 25 should be more accurate. We also verified the measured the spectrum using a separate 1064nm etalon spectrometer (the red dashed curve), and these results are in good agreement with those obtained from the FROG.

### 5.5.3 Measuring Amplified Pulses

In the previous section we demonstrated that our FROG works well. The next step was to begin to measure amplified pulses and see the effects of nonlinearities from the fiber amplifier. We used the single-stage amplifier shown in Figure 1.

As a first step, we measured the spectra of the amplified pulses using our 1064nm etalon spectrometer. We made this measurement before (see Figure 2), but using a much lower resolution spectrometer ( $\sim 0.1\text{nm}$ ) and found that the spectrum did not measurably change as we amplified the pulses by as much as 15 times. However, with the higher spectral resolution (about 1 pm or 100 times better), the spectra shown in Figure 26 look very different.

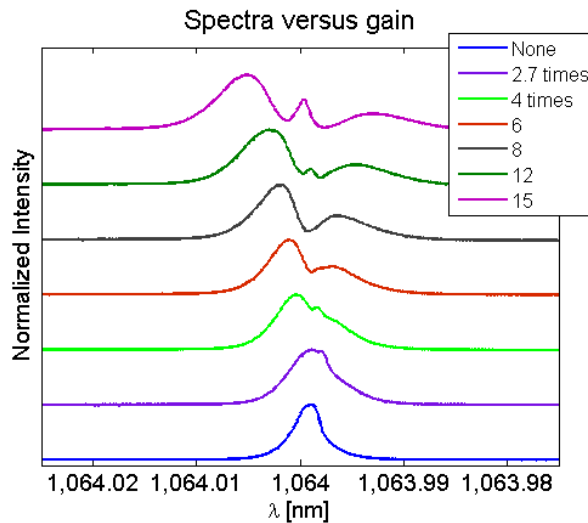


Figure 26. High-resolution spectra ( $\sim 0.09\text{pm}$ ) of the amplified pulse at different pump power levels

The purple spectrum was obtained using 0.5 Watts of pump power (the laser’s output, not accounting for loss coupling loss) and each successive curve corresponds to an additional 0.5 watts. Interestingly, spectral broadening is seen for as little as  $4\times$  gain, and by  $15\times$  gain, the spectrum has changed significantly.

Next we made FROG measurements of the amplified pulses and two of these measurements are shown in Figure 27. To test our measurements, we compared the spectrum retrieved from the FROG trace to that measured with the 1064nm spectrometer and found good agreement between the two. But a spectral broadening and temporal shortening are present in the FROG traces. At 12 times gain, the FWHM of the temporal intensity was around 270ps, and the seed laser pulse duration is 720ps.

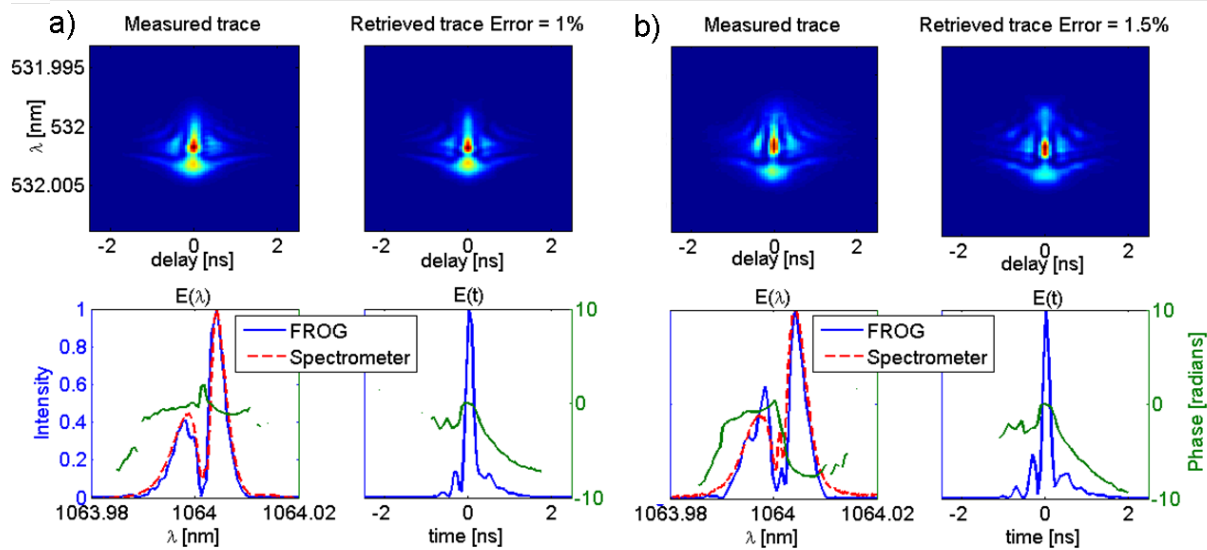


Figure 27. FROG retrieval results for the amplified seed pulse with 8 (a) and 12 times gain (b)

## 5.6 Elegant Single-Shot ns-FROG

We have shown that the pulse-front tilt from an etalon yields a sufficient delay range to make a single-shot ns-FROG. And above, we showed some successful single-shot FROG measurements and the extracted temporal intensity and phases of even amplified pulses. While the experimental setup in Figure 24 works well, we realized that it can be further simplified and made more elegant, so that it is easier to use and less alignment sensitive. This is important because others less skilled in pulse measurement than we are will likely use this device. Therefore in this section we describe and demonstrate our final design for the single-shot ns-FROG.

### 5.6.1 New Experimental Setup

The schematic in Figure 33 illustrates this simplified scheme for making single-shot ns-FROG measurements.

This design uses a Fresnel biprism to split the beam into a pair of crossing beams (rather than using a beam splitter and mirrors). This simplifies the alignment significantly. Next a lens causes the beams to propagate towards each other and to focus at the two gaps of a VIPA etalon. If the focal length of the lens, the apex angle of the biprism, and the spacing between the lens and etalon are all correct, then two highly tilted, but inverted, pulse fronts emerge from the etalon (the dark red lines). As before, several orders emerge from the etalon, even though we align it so that most of the energy is in the order that we desire. If multiple orders are present, then the pulse front will be quite complicated (there will be several pulse fronts each having different tilts), so we use a spatial filter to remove the extra orders. The lenses of the spatial filter also image the tilted pulse fronts onto the second harmonic crystal, so that delay is mapped to position and we obtain a single-shot autocorrelation, but with *nanoseconds* of temporal range. It would be possible to spatially filter and image using a single lens. But using the telescope instead results in collimated beams at the crystal, and the generated autocorrelation signal is also collimated making it easier to image onto the camera through the 532nm etalon. The autocorrelation signal

is then sent to a 532nm etalon imaging spectrometer to generate the FROG trace, just as in our previous single-shot ns-FROG.

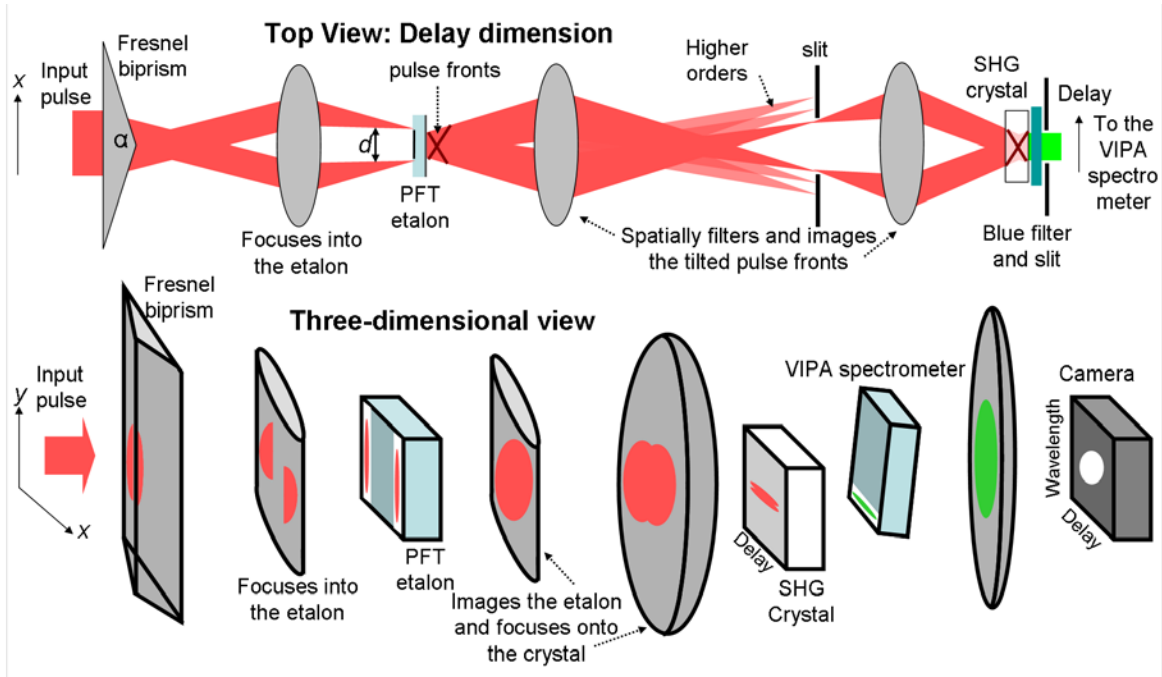


Figure 28. Final version of our single-shot ns-FROG

Figure 5 shows a close up of how the tilted pulse fronts are generated.

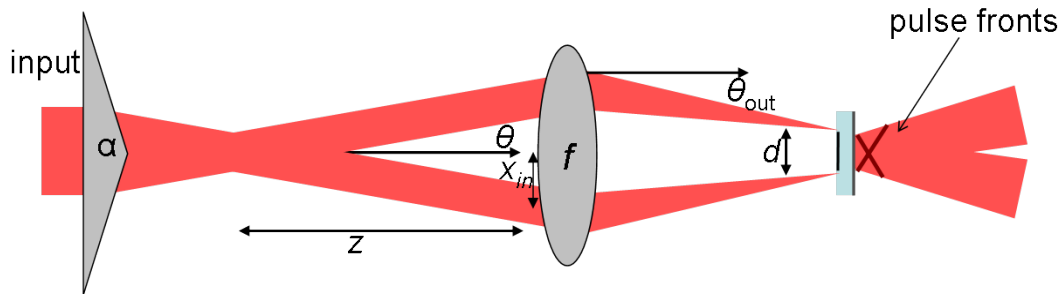


Figure 29. Generating two spatially overlapping oppositely tilted pulse fronts

We choose the biprism apex angle ( $\alpha$ ) and distance between it and the lens (or  $z$ ), so that the spacing between the two beams at the etalon, and their angle into the etalon ( $\theta_{out}$ ), are appropriate. Using ray tracing we find the following formulas for  $d$  and  $\theta_{out}$ :

$$d = 2f\theta \quad (10)$$

$$\theta_{out} = \frac{x_{in}}{f} + \theta \quad (11)$$

The angle into the etalon should be  $1^\circ$  and a 115mm focal length lens will give the needed angular divergence at the etalon. Using these two constraints we find that  $\theta$ , or the half crossing angle produced by the Fresnel biprism should be  $4.98^\circ$ . This can be produced with a  $160^\circ$  apex angle [the crossing angle is given by  $(\alpha-\pi/2)(n-1)$ ]. To obtain the correct incidence angle at the etalon, the distance between the beams' crossing point and the lens can be adjusted. A distance of  $z = 95\text{mm}$ , or  $x = 8.5\text{mm}$ , should result in the required angle.

Note that if a cylindrical lens having exactly the needed focal length is not available, the distance  $d$  and the distance between the etalon and the lens can be adjusted to achieve the correct incidence angle and spacing between the two beams. These are the two most critical parameters, which must be correct in order to efficiently insert both beams into the etalon, and to get the most energy into one order after the etalon. Of course if these two distances are adjusted then the etalon will not be exactly at the focus of the beams, which is still fine as long as the input beams are small enough to fit through the transparent gaps (as much as 5 centimeters away from the focus can be acceptable). In practice, during this early stage of this research, we find that it is useful to mount the cylindrical lens and the etalon to two  $z$ -translation stages. Then the etalon is placed a normal incidence, and the lens is adjusted to choose the correct incidence angle into the etalon, and the etalon is translated to meet the beams when their spacing matches the size of the front coated surface.

### 5.6.2 Testing the Elegant Single-Shot ns-FROG

We bought two custom two-gap etalons from CVI, one with a 5mm thickness and one with a 10mm thickness. We used the 10mm thick etalon to construct the FROG shown in Figure 28. As usual, our first test was to measure a double pulse and the output of the seed laser. These results are shown in Figure 30. For the seed-laser measurement we compared the spectrum retrieved from the FROG to that measured with an independent etalon spectrometer, and the two are in good agreement. The measured temporal duration of 720ps with a spectral bandwidth of 2pm are the same results that we obtained with the first, less elegant version of the single-shot ns-FROG (see Figure 25).

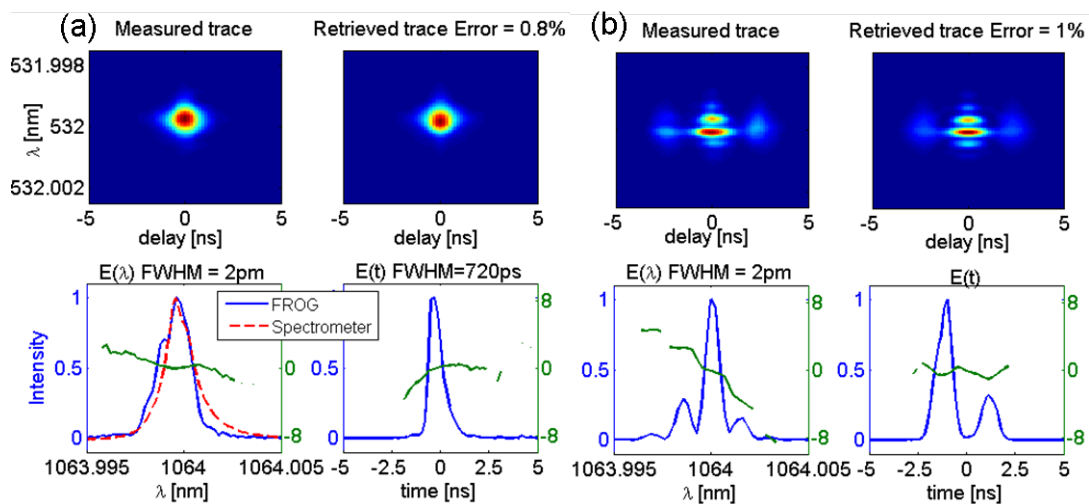


Figure 30. FROG measurement results for a single pulse (a) and a double pulse (b)

The double pulse was generated by sending the 720ps pulses into a Michelson interferometer with a path length difference of 2.57 ns to form a double pulse. The results of this measurement are shown at the right of Figure 30. For this double pulse we expected a temporal peak ratio of 36%, which is in good agreement with what we measured. We also measured two other double pulses with different temporal spacing, and the summary of all of these measurements is shown in Figure 31. In each of these FROG retrievals, the differences between the retrieved and measured traces were 1% or less, indicating that the algorithm converged well. These temporal spacing between the pulses are 3ns (top), 2.56ns (middle), and 2ns (bottom). In all of these cases, the relative peak heights should be 36%. For the two shorter pulses, we measured this correctly, but for the 3ns pulse, the second peak is a little too weak (~25%) because the temporal fringes are faster and therefore more difficult to resolve.

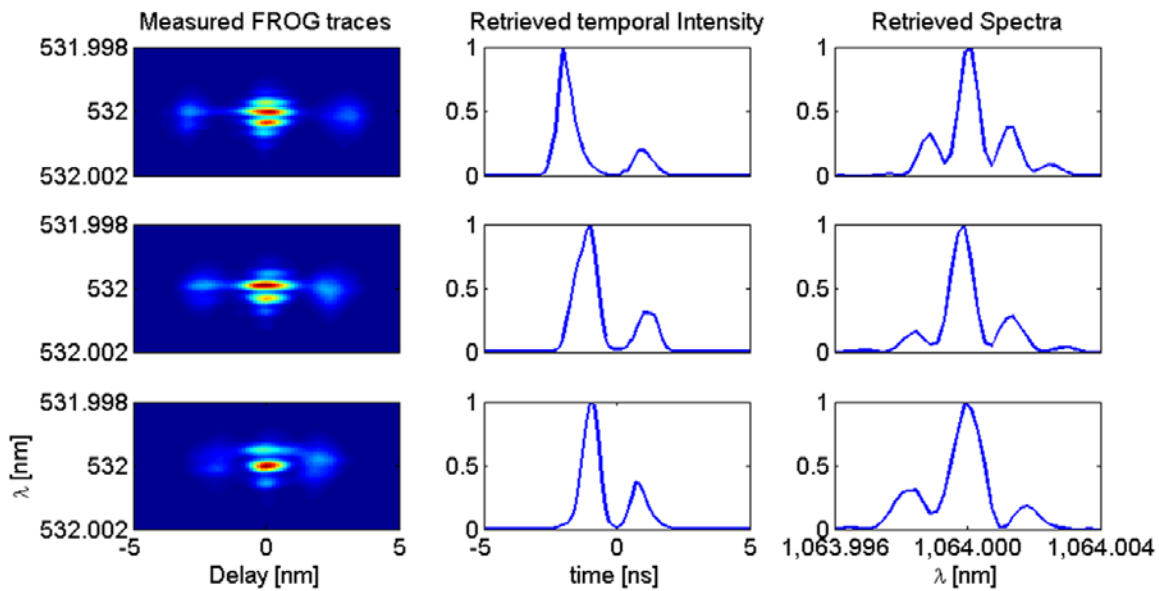


Figure 31. FROG measurements of 3ns (top), a 2.56ns (middle), and a 2ns double pulse (bottom)

### 5.6.3 Measurement Range of Our Single-Shot ns-FROG

Using the measured spectral resolution of the 532nm (see Figure 13) etalon and what we know about the pulse front tilt (see Section 5.4), we can estimate the parameters for our FROG.

Spectral Resolution	Spectral Range	Temporal Resolution	Temporal Range	Maximum time-bandwidth product	Measurable pulses at 1064nm
0.37pm (~4ns)	27pm (~60ps)	130ps or 60ps	8.5ns or 1.8ns	~30	from 130ps to 4ns or from 60ps to 1.8ns

Table 2. Summary of pulses measurable with the single-shot ns-FROG.

For a center wavelength of 1064nm, these are shown in Table 1.

Because the tilt of the pulse fronts at the SH crystal can be varied, the maximum and minimum resolvable temporal features of the FROG are limited by the 532nm etalon spectrometer. The etalon spectrometer's free spectral range determines the maximum bandwidth or equivalently the smallest temporal features that the pulse can have. This is 10pm for the second harmonic, and is  $2\sqrt{2}$  larger or 27pm for the input 1064nm pulse. The etalon's line width (spectral resolution) determines the largest measurable temporal features which is 4ns for the 1064nm pulse or  $\sim 6.3$ ns for the second harmonic (which is  $\sqrt{2}$  longer than the fundamental). But the maximum measurable time-bandwidth product (TBP) is limited by the delay axis of the FROG, due to the long depth of field needed to image the crystal through the 532nm etalon, and this is 30 (for a 2cm wide crystal). Because this time bandwidth product is about  $\frac{1}{2}$  of the finesse of the 532nm etalon spectrometer, two possible configurations of the FROG are possible: one that measures pulses ranging from 130 to 4000ps and one that ranges from 60 to 1800ps. By using a wider crystal (the aperture width, not the thickness), the measurable TBP could be increased.

In conclusion, the main limitation of our FROG is the need to image through the spectrometer's etalon, which requires a large dept of field, or limits the smallest resolvable temporal feature. After this, the next limitation is the finesse of the 532nm etalon which can probably be no greater than  $\sim 90$ .

#### 5.6.4 Measuring amplified pulses

Now that we are confident in our new single-shot ns-FROG, we returned to studying the pulses from our single-stage Yb fiber amplifier in order to answer one of the main questions of our project: "Are the temporal intensity and phase of the pulses changing from shot to shot?"

Our single-shot FROG is a powerful tool for watching the pulse change in real time. This is illustrated in Figure 32 which shows how the FROG trace changes as we increased the 976nm pump power from 1.2 to 2.8 Watts, or vary the gain from about 8 to 15 times. The nonlinearities, which are probably a combination of self-phase modulation and Raman scattering, increase as the pump power is increased. This results in a red-shifted and broadened spectrum and also smaller temporal features.

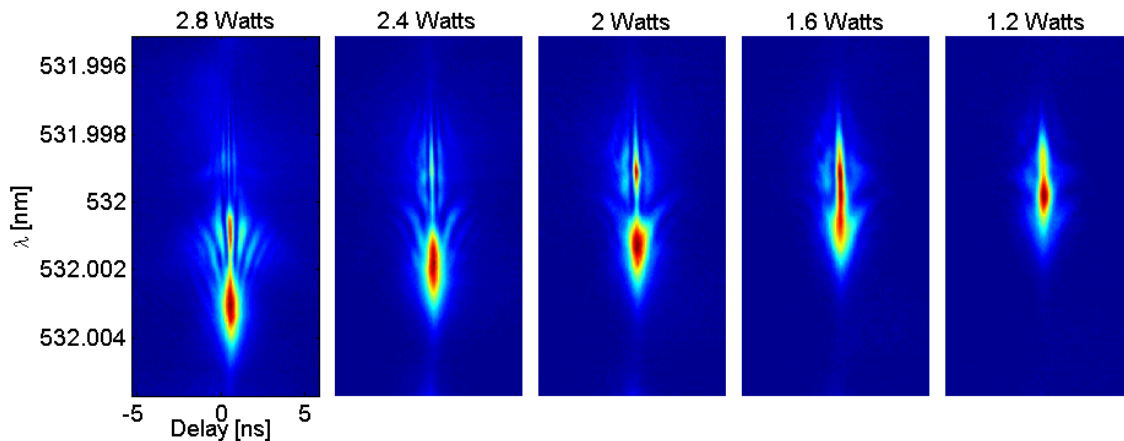


Figure 32. FROG traces of pulses from the Yb fiber amplifier for different pump power levels

Figure 33 shows retrievals for two of these pulses. The results on the left were for a pump power of 2 Watts (170mW average power, or 12× amplification) and those on the right were with 2.8 watts (213mW average power of 15× amplification). The red spectrum was measured with the 1064nm etalon spectrometer. It is in pretty good agreement with the FROG spectrum, but note that the FROG’s etalon has a narrower line width (0.1pm rather than 1pm) than the one that we use in our spectrometer. Also, as we showed previously in Figure 18, because of the oversampling of the FROG trace, the algorithm has the ability to fill in missing spectral resolution. These are probably the reasons for the discrepancies for the 12× amplified pulse. These results are similar to what we measured with our previous version of the single-shot ns-FROG, and again demonstrate that the simplified version works well also.

The results for the 15× amplified pulse are slightly worse, because this pulse is quite complicated and at the edge of our measurement capabilities with this FROG. Specifically, its bandwidth is larger than the free spectral range of our 10mm 532nm etalon, so the shorter wavelengths may be getting slightly attenuated. But remarkably, the retrieved spectrum is still quite similar to the independently measured spectrum, and some of the smaller spectral features may have been correctly added in by the FROG algorithm.

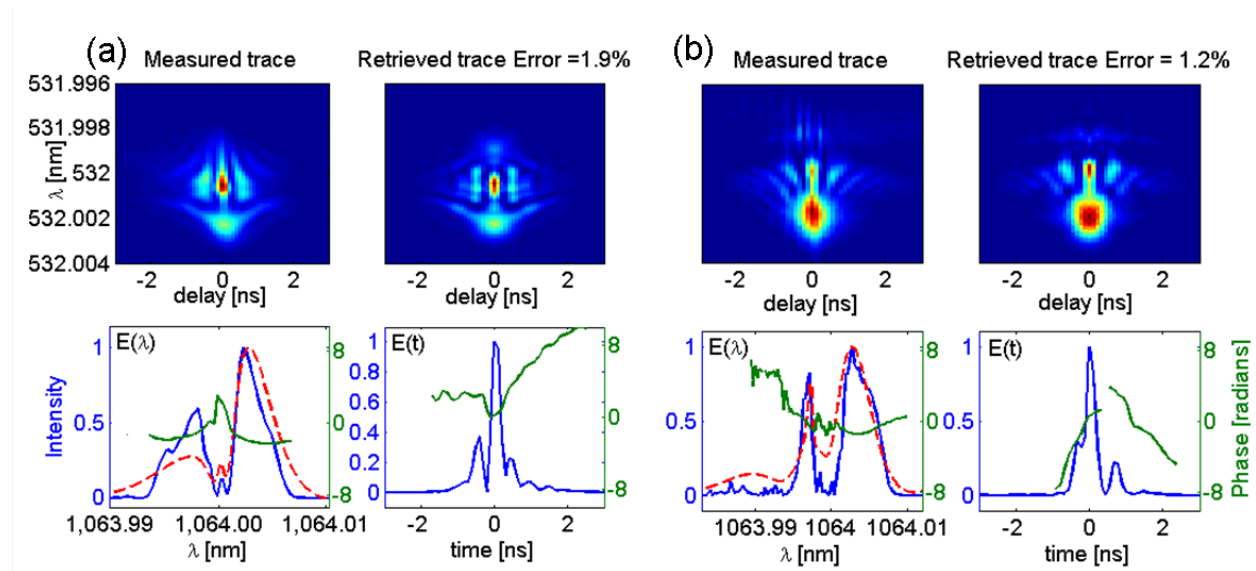


Figure 33. FROG retrieval results for 12× (a) and 15× amplification (b)

The remaining question of our project is to determine whether or not the temporal intensity and phase of the amplified pulses are varying from shot-to-shot in the 10kHz pulse train. In a first attempt to answer this question we made single-shot spectra measurements of the amplified pulses using the 1064nm etalon spectrometer. These are shown in Figure 34.

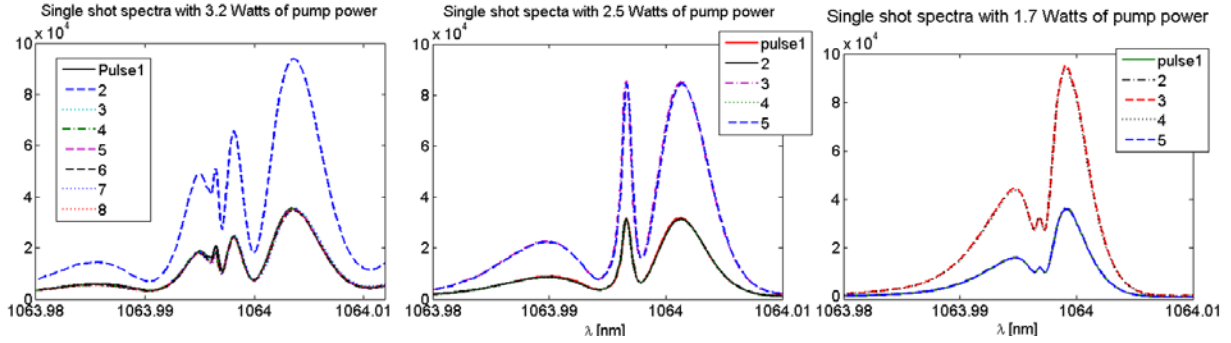


Figure 34. Single shot spectra of the amplified pulses at 3 different pump powers

Each of these plots contains several single shot spectra at 3 different pump power levels. While some variation in the overall power of the amplified pulses was seen, the shape of the spectrum remained constant. The spectra shown were measured over about a minute, to also ensure that there were no slower variations. The varying power of the amplified pulses could be due to several factors, such as an unstable repetition rate or jitter in the seed laser. But power variations from pulse to pulse should not be a serious limitation for coherent combination and can probably be easily overcome by using a different seed laser if necessary.

The stable spectral shape indicates that the temporal intensity and phase of the pulse are probably also stable as well. But to check this we can look at *single-shot* FROG traces, which depend on all of these parameters. In the past, our FROG measurements were averaged over 10-100 pulses in the pulse train in order to obtain a bright enough trace at the camera. But, when amplifying significantly, we have enough signal to see the FROG trace of a single pulse. Several single-pulse FROG traces are shown in Figure 35.

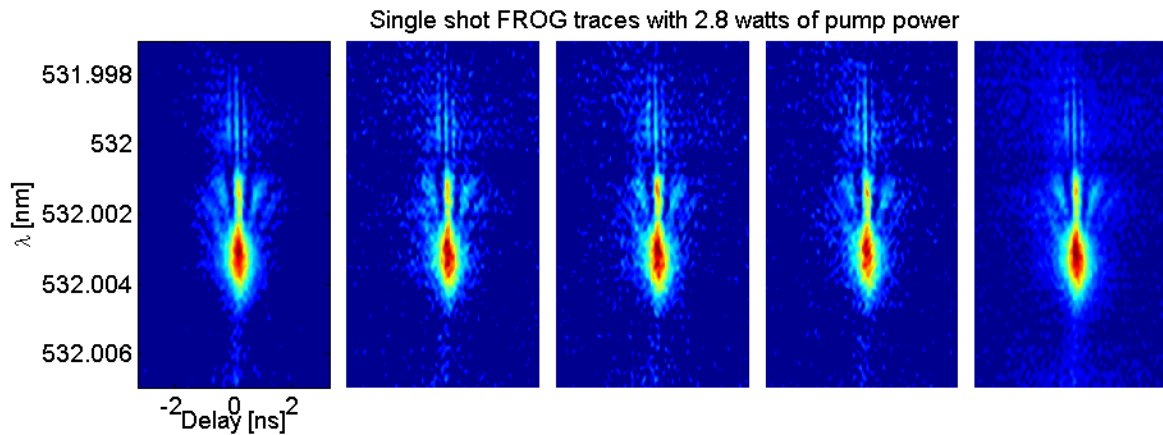


Figure 35. Single-shot FROG traces of an amplified pulse

Although these traces are a bit noisy (even after Fourier filtering and background subtraction), it is evident that their shape (rms difference  $< \sim 1\%$ ) is not changing significantly from shot to shot. This indicates that the temporal field of the amplified pulses, at least up to a gain of around 15 times, is stable from pulse to pulse in the pulse train, which is good news for coherently combining them.

Retrievals for two of the single shot measurements are shown in Figure 36. The FROG error for these retrievals is a little higher than usual due to the noise in the measurements, but nevertheless, the retrieved spectra are in pretty good agreement with those measured with a spectrometer. Also, the retrieved pulse shapes from the two retrievals are very similar with the difference probably being due to the noise in the measurements. Again these measurements are at the edge of the capability of our FROG due to the bandwidth of the pulses.

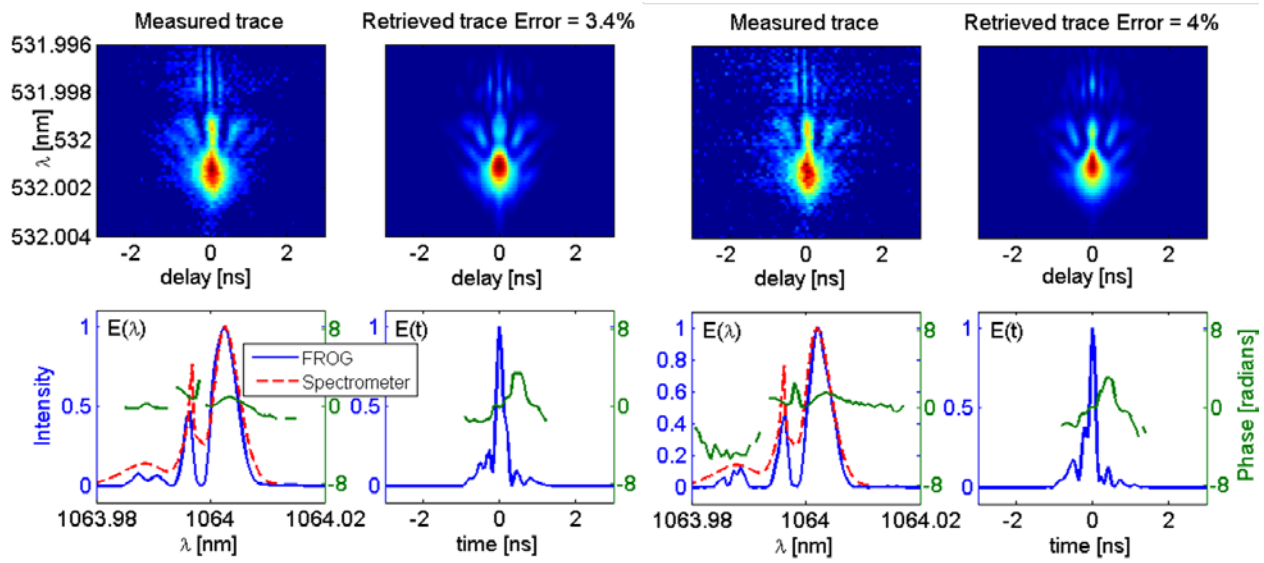


Figure 36. Retrievals for two different single shot FROG measurements

## 6. Conclusions

We achieved our main goal of developing a single-shot ns-FROG. We were even able to do so in a compact and simple manner, so that this device will be practical to use and well suited for commercialization. The FROG shown in this report can measure pulses ranging in duration from 130ps to 4ns, or 60ps to 1.8ns. We demonstrated the FROG by measuring double pulses and the seed laser for our amplifier.

We have further demonstrated our FROG by making measurements of the amplified pulses. The FROG traces nicely show in real time how the pulse shape changes as the pump power is increased. We have also been able to make single-pulse FROG measurements of more intense amplified pulses, which indicate that both the temporal intensity and phase remain constant for each pulse in the pulse train.

Our study indicates that coherent combination seems feasible with an amplifier such as the one that we have built. Our measurements show that the absolute phase drift was less than one radian per second (for 13dB of gain), and these FROG measurements show that the pulse shape is stable from shot to shot. It would be interesting to add additional stages of amplification using large mode area photonic crystal fibers and measure FROG traces of these pulses. Perhaps in this case, there will be shot-to-shot fluctuations of the temporal pulse shape. It will also be very interesting to try coherent combination and see how the FROG traces look for the combined pulses.

In any case, the FROG that we have developed should be very useful for indicating that two lasers are indeed operating as one.

## 7. References

1. K. T. Vu, A. Malinowski, D. J. Richardson, F. Ghiringhelli, L. M. B. Hickey, and M. N. Zervas, "Adaptive pulse shape control in a diode-seeded nanosecond fiber MOPA system," *CR Phys* **7**, 170-176 (2006).
2. B. Braun, F. X. Kärtner, U. Keller, J. P. Meyn, and G. Huber, "Passively Q-switched 180-ps Nd: LaSc<sub>3</sub> (BO<sub>3</sub>)<sub>4</sub> microchip laser," *Opt. Lett.* **21**, 405-407 (1996).
3. C. Brooks and F. Di Teodoro, "1-mJ energy, 1-MW peak-power, 10-W average-power, spectrally narrow, diffraction-limited pulses from a photonic-crystal fiber amplifier," *Opt. Express* **13**, 8999-9002 (2005).
4. C. D. Brooks and F. Di Teodoro, "Multimegawatt peak-power, single-transverse-mode operation of a 100 m core diameter, Yb-doped rodlike photonic crystal fiber amplifier," *Appl. Phys. Lett.* **89**, 111119 (2006).
5. F. Di Teodoro and C. D. Brooks, "1.1 MW peak-power, 7 W average-power, high-spectral-brightness, diffraction-limited pulses from a photonic crystal fiber amplifier," *Opt. Lett.* **30**, 2694-2696 (2005).
6. R. Trebino, *Frequency-Resolved Optical Gating: The Measurement of Ultrashort Laser Pulses* (Kluwer Academic Publishers, Boston, 2002).
7. H. Stark, ed., *Image Recovery: Theory and Application* (Academic Press, Orlando, 1987).
8. E. Zeek, A. P. Shreenath, M. Kimmel, and R. Trebino, "Simultaneous Automatic Calibration and Direction-of-Time-Ambiguity Removal in Frequency-Resolved Optical Gating," *Appl. Phys. B* **B74**, S265-271 (2002).
9. Y. Mairesse and F. Quéré, "Frequency-resolved optical gating for complete reconstruction of attosecond bursts," *Phys Rev A* **71**, 011401 (2005).
10. G. Sansone, E. Benedetti, C. Vozzi, S. Stagira, and M. Nisoli, "Attosecond metrology in the few-optical-cycle regime," *New J. Phys.* **10**, 025006 (2008).
11. J. R. Birge, R. Ell, and F. X. Kärtner, "Two-dimensional spectral shearing interferometry for few-cycle pulse characterization," *Opt. Lett.* **31**, 2063-2065 (2006).
12. H. Fuchs, D. Woll, T. Ulm, and J. A. L'Huillier, "High resolution FROG system for the characterization of ps laser pulses," *Applied Physics B (Lasers and Optics)* **88**, 393-396 (2007).
13. M. Born and E. Wolf, *Principles of Optics*, 7 ed. (Cambridge University Press, New York, 1999).
14. M. Shirasaki, "Large angular dispersion by a virtually imaged phased array and its application to a wavelength demultiplexer," *Opt. Lett.* **21**, 366-368 (1996).
15. C. Dorrer, "Influence of the calibration of the detector on spectral interferometry," *J. Opt. Soc. Am. B* **16**, 1160-1168 (1999).
16. V. J. Coates and H. Hausdorff, "Interferometric Method of Measuring the Spectral Slit Width of Spectrometers," *J. Opt. Soc. Am.* **45**, 425-430 (1955).
17. V. N. Kumar and D. N. Rao, "Determination of the instrument function of a grating spectrometer by using white-light interferometry," *Appl. Opt.* **36**, 4535-4539 (1997).
18. P. Bownan, P. Gabolde, M. A. Coughlan, R. Trebino, and R. J. Levis, "Measuring the spatiotemporal electric field of ultrashort pulses with high spatial and spectral resolution," *J. Opt. Soc. Am. B* **25**, A81-A92 (2008).
19. S. Akturk, X. Gu, P. Gabolde, and R. Trebino, "The general theory of first-order spatio-temporal distortions of Gaussian pulses and beams," *Opt. Express* **13**, 8642-8661 (2005).
20. C. Dorrer, E. M. Kosik, and I. A. Walmsley, "Spatio-temporal characterization of the electric field of ultrashort optical pulses using two-dimensional shearing interferometry," *Applied Physics B (Lasers and Optics)* **74**, 209-217 (2002).

21. Z. Bor, B. Racz, G. Szabo, M. Hilbert, and H. A. Hazim, "Femtosecond pulse front tilt caused by angular dispersion," *Opt Eng* **32**, 2501-2504 (1993).
22. J. Hebling, "Derivation of the pulse front tilt caused by angular dispersion," *Optical and Quantum Electronics* **28**, 1759-1763 (1996).
23. C. Froehly, A. Lacourt, and J. C. Vienot, "Time Impulse Responce and time Frequency Responce of Optical Pupils," *Nouvelle Revue D'Optique* **4**, 183-196 (1973).
24. D. Meshulach, D. Yelin, and Y. Silberberg, "Real-Time Spatial-Spectral Interference Measurements of Ultrashort Optical Pulses," *J. Opt. Soc. Am. B* **14**, 2095-2098 (1997).
25. P. Bowlan, P. Gabolde, A. Schreenath, K. McGresham, R. Trebino, and S. Akturk, "Crossed-beam spectral interferometry: a simple, high-spectral-resolution method for completely characterizing complex ultrashort pulses in real time," *Opt. Express* **14**, 11892-11900 (2006).
26. J. P. Geindre, P. Audebert, S. Rebibo, and J. C. Gauthier, "Single-shot spectral interferometry with chirped pulses," *Opt. Lett.* **26**, 1612-1614 (2001).
27. K. Misawa and T. Kobayashi, "Femtosecond Sangac interferometer for phase spectroscopy," *Opt. Lett.* **20**, 1550-1552 (1995).
28. J. W. Goodman, *Introduction to Fourier optics* (Roberts & Co, 2005).
29. S. Xiao, A. M. Weiner, and C. Lin, "A dispersion law for virtually imaged phased-array spectral dispersers based on paraxial wave theory," *IEEE J. Quantum Electron.* **40**, 420-426 (2004).
30. P. Gabolde, D. Lee, S. Akturk, and R. Trebino, "Describing first-order spatio-temporal distortions in ultrashort pulses using normalized parameters," *Opt. Express* **15**, 242-251 (2007).

## List of Acronyms, Abbreviations, and Symbols

Acronym	Description
FROG	frequency-resolved optical gating
MOFA	master oscillator fiber amplifier
PFT	pulse-front tilt
SHG	second-harmonic generation
SI	spectral interferometry
TBP	time-bandwidth product
TI	temporal interferometry
VIPA	virtual image phase array
YDFA	ytterbium-doped fiber-amplifier